VI ENGINEERING PHYSICS

VI.1 Flow of Cooling Media

Fiber formation is always connected with handling of fluid flow of one sort or another. In the case of formation from melt, the filaments must be cooled. This is done mostly with the help of air, though on rare occasions a liquid (water) may be used. In cases of formation from solution, it is necessary to use either air for dry processes or liquids for wet processes. In every case, the questions of fluid dynamics is of major interest.

Occasionally, air is used as a means of transporting fibers. In some processes, aerodynamic drag is used as means to generate drawing force. Such processes are most often used in spunbonded processes. If a spunbonded process uses mechanical transport, air jets are applied for depositing the fibers on the conveying belts. The air flow in the equipment for fiber transport is somewhat more complex than in cooling problems.

VI.1.a Quench Systems

For fiber cooling, the air flow is applied either in *cross flow* or in *co-current flow*, which is some times called *radial flow*. In cases of dry formation from solution, the drying air (or neutral gas) is applied either in *co-current* or in *counter current*. The last system is used in formation from melt only exceptionally. In formation from melt, perhaps the most frequent is *cross flow* mode; this is the oldest system and still very popular.

An example of the realization of cross flow quench is given in figure VI.1. Previously conditioned to temperature and proper humidity, the air is introduced into a flow distribution chamber, A. The air stream is then directed perpendicularly to the filaments. Before the air reaches the fibers, however, it passes through a flow equalization honey comb layer, or layers, E, to force the air into a parallel flow. Sometimes honey comb is replaced with thick metal plates that have a plurality of holes. This is a less expensive method, but is "aerodynamically not recommended". Behind the honey comb, at least one layer of fine mesh screen should be placed to remove any vorticity from the air. More sophisticated, highly recommended equipment has the air introducing equipment segmented. The segments are provided with individual flow regulators, R, consisting of louvers or plates with mismatched holes. The last possibility appears aerodynamically more favorable. In the really elaborate systems, each segment may have individual temperature control. Plates, P, parallel to the axis of filament travel, are usually placed in order to guide the stream of flowing air to avoid unnecessary turbulence which may be caused by room drafts and by a pumping action of the moving filaments.

Figure VI.1 also shows a provision for the removal of fumes, D, emanating from the hot fibers and consisting of byproducts of polymer degradation and evaporat-

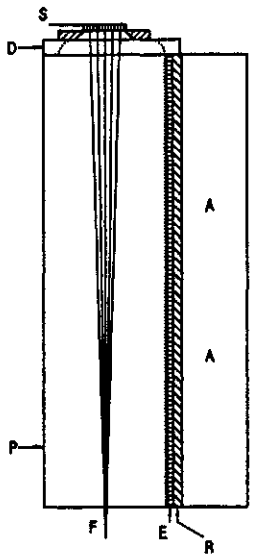

Figure VI.1: *Cross flow quench, with air flow perpendicular to the filaments. Explanation in text.*

ing or subliming additives, e.g. stabilizers. The fume removal arrangement is not a part of the quench system, but it usually does affect the work of the system. The majority of fumes is generated where the fibers are the hottest, close to the spinnerette, and therefore a "bar" or "ring" with applied suction is located as closely under the spinnerette as possible. The aspirated smoke must be led as early as possible through some condensing, dust retention, or absorbing equipment to remove the pollutants from the air before it is discharged back into the atmosphere. The suction may potentially influence the pattern of quench air flow. Good precautions should be taken that the cold air aspirated by the fume removal does not bounce off the spinnerette surface. With incompletely efficient fume removal, bouncing off spinnerette face included, some of the fume components may become deposited on the spinnerette surface. This requires cleaning, and this, in turn, diminishes the effective operating time.

The fume removing bar, square, or ring consists of a pipe with either a round or rectangular cross section, ranging from two to a maximum of ten centimeters in diameter and provided with a slot through which the air surrounding the fibers is aspirated. Only rarely is the fume removal supplied with air of its own; mostly it operates on "stolen" quench air.

In large commercial processes, all of the air used for quenching must be removed. The design of this is not very difficult, but care must be taken not to alter the intended quench pattern. The separate fume removal is necessary, as it is easier to purify a smaller volume of air. The importance of the fume removal to environmental protection is obvious. Design of this area should be treated care-

fully as air flow disturbances in this zone may very adversely affect the quality of fibers, especially their uniformity.

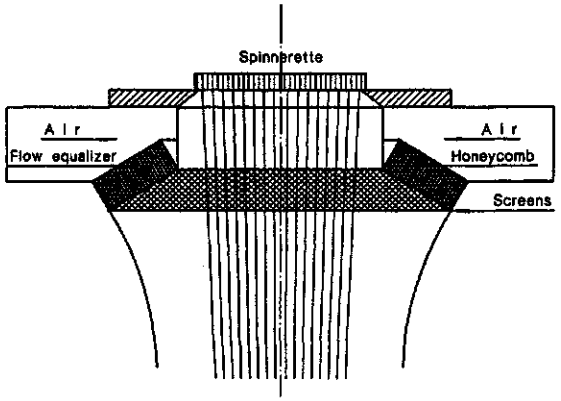

Figure VI.2: *Co-current quench, one of possible solutions for air introduction. Explanation in text.*

The parallel flow quench systems, sometimes called "radial systems", are usually preferred for processes utilizing round spinnerettes of 500 to 1500 filaments where there exists a concern about high fiber to fiber uniformity. The cooling air is introduced from a circumferential orifice inward, radially toward the center of the filament bundle. Naturally, non-circular spinnerettes do not prohibit the use of co-current quench. In the case of rectangular spinnerettes, the geometry would have to be changed to linear, most likely with two bars instead of a circular arrangement. In standard engineering terminology we are speaking about an axial - co-current system. The air should flow parallel to the axis of filament travel. The stream of air and fibers is usually contained within a pipe, often circular, the diameter of which, naturally, depends on the size of spinline and volume of air.

It proves to be difficult to design the orifice introducing the quench air for parallel flow. One of the possible solutions for circular spinnerettes is given in figure VI.2. The air is preferably introduced through at least two tangentially located inlet pipes to assure good air distribution in the circular main channel. The resulting circular motion of the air is broken by the equalizers, consisting of a bent honeycomb or a large number of capillary like holes drilled in a circular partition. Though the threadline comes in contact with the quenching air with some delay, the geometry of this solution allows the use of relatively high air velocities without causing appreciable disturbances of the threadline. Other possible solutions permit an earlier exposure of fibers to the quenching air, but they are more vulnerable to formation of air turbulence. On the other hand, delay of quench is a good technique applied often on purpose, and in such cases the delay may be many times larger than the necessary delay inherent to the design in figure VI.2.

An interesting solution for a co-current quench has been offered by Fuji-Filter Co. Cooling air is led between the walls of a double walled tube. The inner wall is made of slots inclined to direct the air stream radially. The initial angle of the air travel is around 75° in relation to the fiber path. The cooling air is introduced

from the bottom of the double walled tube which surrounds the fibers as they exit from the spinnerette.

There is no question, cross flow quench is more efficient and it offers relatively easy ways of *profiling* the flow intensity, as well as temperature along the filament path. As the negative points one must give the bellowing of the spinline, especially with higher intensity flow and with longer quench zones. In cases of large multi-filament spinlines, the air must pass through a large number of fiber rows, and as a result, the air flow intensity rapidly decreases and the temperature increases for each following row. This leads to a large gradient in quality of the fibers due to the unavoidable gradient in cooling intensity.

The co-current quench gives substantially better cooling uniformity, but overall quench efficiency is smaller, unfit for profiling. The low cooling efficiency may require intensive flow and this, in turn, on occasions may create excessive drag force on the fibers, thereby contributing to filament breaks.

Substantial increase in cooling intensity, as compared with co-current flow, may be obtained with a counter-current system. The air introduction is located at the level of exit of fibers. It does not require so careful a design since at this point the fibers have higher velocity and are not so fragile. Removal of the spent quench air close to the spinnerette is the critical point. Lacing up of a spinning position requires that the quench air be closed. Filament breaks create more unforgiving situations. Profiling of cooling intensity is also impossible. For dry formation from solution, in turn, this is the preferred solution.

VI.1.b Fluid Dynamics

In fiber formation from melt, in the quench zone the fibers exchange heat with the flowing air, hence air temperature is changing. As a matter of fact, in the dry formation from solution we have a similar situation, except that instead of air we have air with a changing concentration of solvent vapors in addition to changing temperature of air. All this means that there is a certain interaction between the moving filaments and the moving fluid.[1]

If we consider cross flow quench system, then the air is, in principle, perpendicular to the moving fibers. We say "in principle" because the fibers converge from a maximum of the diameter of the spinnerette hole pattern down to practically zero on the take up rollers or on a converging guide. In effect, we have a certain angle, usually not exceeding some 5°, perhaps 7°, between a fiber and the system axis, and the angle varies within the fiber tow. On occasions, the air may be guided under an angle somewhat different than 90°.

An object located in a stream of fluid is subject to drag forces. If we consider a fiber as a cylinder located in a stream of air then the drag exerted on the cylinder is proportional to the velocity component normal to the cylinder axis, which in figure VI.3 is designated v_n. In case that the air attacks the cylinder at an angle λ, the normal velocity component will be:

$$v_n = v \sin \lambda \tag{VI.1}$$

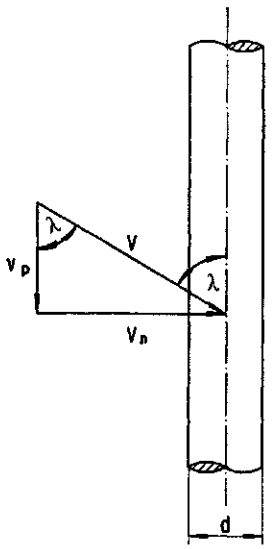

Figure VI.3: *Distribution of fluid velocities in cross flow.*

The flow of a fluid around the cylindrical obstacle depends on the magnitude of the Reynolds number calculated in relation to the cylinder diameter, d. The Reynolds number is given by

$$Re_d = \frac{v_n d}{\nu} \tag{VI.2}$$

where ν is kinematic viscosity of the fluid.*

Figure VI.4 shows schematically different patterns, depending on Reynolds number, of flow around a cylinder. In the figure, Case A corresponds to a laminar flow, case B is at the high limit of laminar flow, case C represents a turbulent flow which is considered[2] to take place above $Re_d > 10^5$. From figure VI.4 one may expect that the pressure around the cylinder should not be equal. Indeed, as shown in bottom of figure VI.4, the pressure, P, varies substantially. According to the potential theory, the pressure around the cylinder depends on the angle ϕ. At the point of incidence the angle is taken as $\phi = 0$.

$$P(\phi) = 1 - 4\sin^2\phi \tag{VI.3}$$

In practice, the pressure deviates rather strongly from that calculated from equation VI.3, and depends to a certain degree on the Reynolds number, as it is evident from figure VI.4. Above the critical value of Reynolds number, 10^5, the flow pattern changes markedly. The pressure differences are responsible, in part, for the drag, as well as for the bellowing. The magnitude of the pressure drag, D, per unit of cylinder length is given by equation VI.4.

$$D = C_D \frac{\rho v_n^2 d}{2} \tag{VI.4}$$

*Data on some physical properties of air are given in the Appendix.

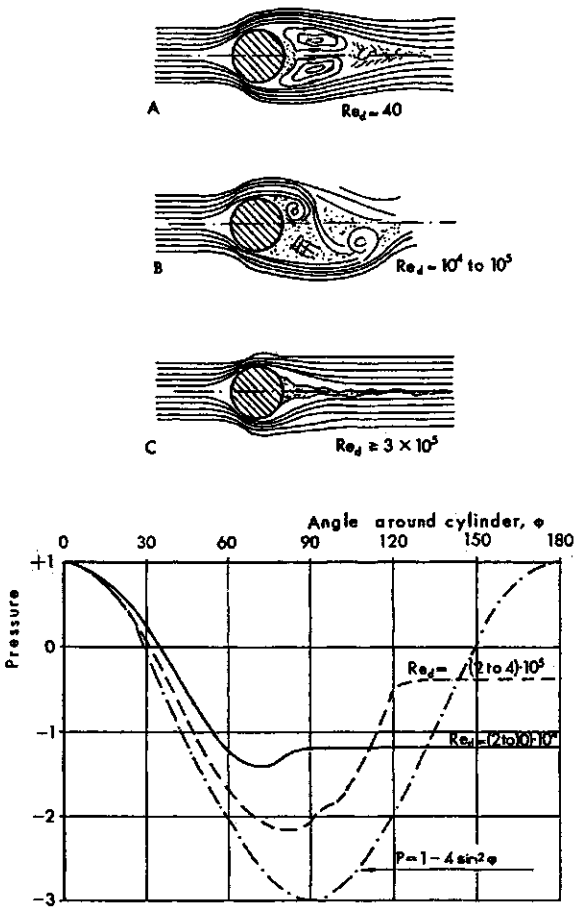

Figure VI.4: *Flow of fluid around a cylinder. Cases A and B laminar flow, case C turbulent flow. Bottom: pressure distribution around the circumference of a cylinder in a perpendicularly flowing stream of gas measured at indicated Reynolds numbers and calculated from equation VI.3. After S. F. Hoerner*[2]

where C_D is the coefficient of pressure drag dependent on the Reynolds number, d is cylinder (fiber) diameter, ρ is density of the fluid (air), and v_n normal component of the fluid velocity.

The magnitude of the coefficient of drag, C_D, in relation to the Reynolds number, Re_d, for a cylinder is shown in figure VI.5. The values may be also calculated with a very good approximation from the following equation, provided that $10^{-2} \leq Re_d \leq 7 \cdot 10^3$:

$$C_D = 9.9785 Re_d^{-0.7723} + 1.2482 Re_d^{-0.0355} \tag{VI.5}$$

The drag for cylinders with non-circular cross sections differs markedly from those with circular cross sections. While the drag coefficient for Reynolds numbers

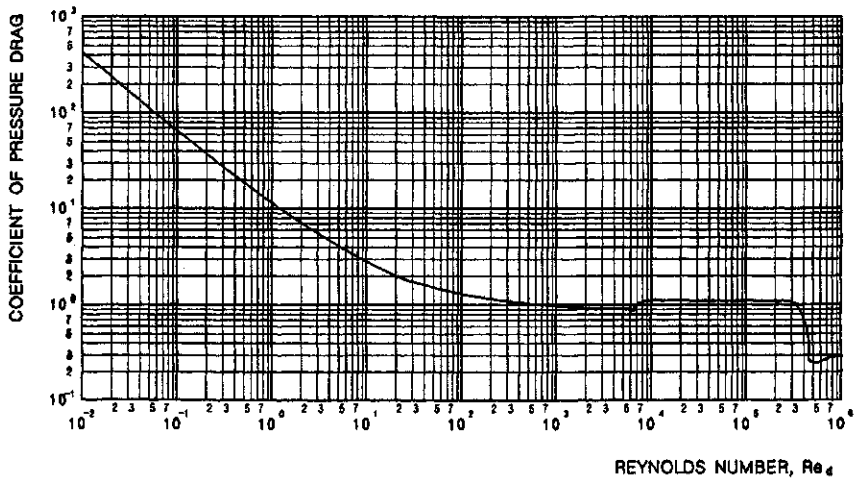

Figure VI.5: *Coefficient of pressure drag in relation to Reynolds number calculated on diameter of a cylinder. After S. F. Hoerner*[2]

10^4 to 10^5 for a circular cylinder is 1.2, for the same range of Reynolds numbers, cylinders with elliptical cross section of 2 : 1 axis ratio $C_D = 0.67$; for even sided triangular cross section with blunt edges $C_D = 1.4$, for a square cross section with blunt edges $C_D = 1.6$.[2]

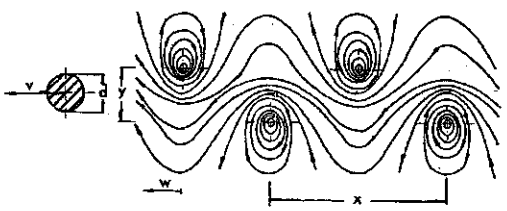

Figure VI.6: *Vortex street resulting from air flow around a long cylinder in transitional flow region. Explanation in text. After S. F. Hoerner*[2]

The perpendicular flow around cylinders may cause one more type of disturbance. The conditions of the transient flow, between laminar and turbulent, (case B in figure VI.4) may produce a so called *vortex street*, which is shown schematically in figure VI.6. The double row of vortices, alternating in their positions, is the reason for the acoustical phenomenon accompanying the vortex street that is called the *Aeolian harp*. The *vortex street* moves with a velocity w, it is some six times smaller than the air velocity, $w/v = 1/6$. The wavelength of the vortex street, x, depends on the diameter of the cylinder, a, and is equal $x = 4.5\ d$. The frequency of the vortices on one side of the street, f, is[3] given by:

$$f = v - w/x \tag{VI.6}$$

In the case when the effect of the "vortex street" would be strong enough to disturb the filaments, fiber nonuniformities might be caused with frequencies which

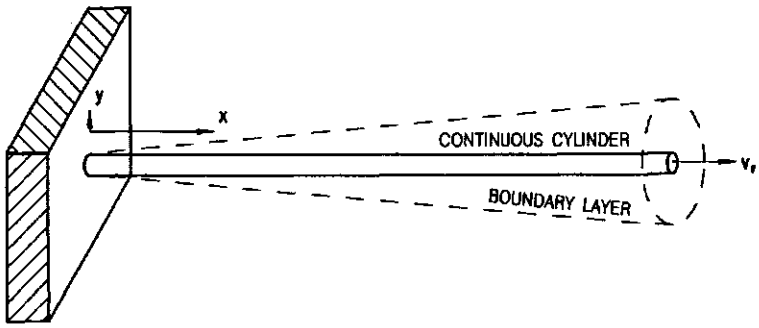

Figure VI.7: *Boundary layer around a moving continuous cylinder.*

could be of concern. If the vortex street is not strong enough to be detrimental to the fiber quality, it must be considered in every multifilament formation since the air flow after passing the first line of filaments is no longer laminar. No theoretical solution of these questions is available.

In the co-current quench system, the air flow is more or less parallel to the axis of the filament travel. The deviation from exactly parallel flow is by as much as is caused by the convergence of the filaments in the spinline. The parallel flow is the cause of frictional drag.

A theoretical solution for the frictional drag and for the boundary layer question for a continuous cylinder has been proposed by B. C. Sakiadis[3]. The boundary layer of a continuous cylinder emerging from a die or capillary, C, as presented in figure VI.7, is different from the boundary layer of a moving cylinder of finite length. In the first case, the boundary layer grows in the direction of motion, while in the latter case the direction of boundary layer growth is opposite.

As a starting point, Sakiadis takes the boundary layer equations for laminar, steady, and incompressible flow on a moving continuous cylindrical surface:

$$v\frac{\partial v}{\partial x} + v_n\frac{\partial v}{\partial r} = \nu\left(\frac{\partial^2 v}{\partial r} + \frac{1}{r}\frac{\partial v}{\partial r}\right), \tag{VI.7}$$

$$\frac{\partial v}{\partial x} + \frac{\partial v_n}{\partial r} + \frac{v_n}{r} = 0 \tag{VI.8}$$

where v is the fluid velocity component in the direction parallel to the cylinder axis x, v_n is the fluid velocity component parallel to the cylinder radius and directed along the y axis, which is normal to the cylinder axis x, r is the cylindrical coordinate from the axis of the cylindrical surface, a is cylinder diameter, and ν is kinematic viscosity of the fluid. The boundary conditions are set as follows: $v = v_f$; $v_n = 0$ at $r = a$; $v \to 0$ at $r \to \infty$. Additionally, it is assumed that

$$\left(\frac{\partial v}{\partial r}\right)_{r=\infty} = 0$$

The boundary conditions assumed for the continuous surface represent the difference in comparison with the solution for a cylinder of a finite length.

The major problem connected with the proposed solution of these equations is the selection of a velocity profile. Sakiadis[3] assumes the following velocity profile:

$$\frac{v}{v_f} = \left[1 - \frac{1}{\beta}\ln\left(1 + \frac{y}{a}\right)\right] \tag{VI.9}$$

where β is a function of x but is not a function of y.

Consequently, Sakiadis derived the following equations for the major parameters connected with the motion of a continuous cylindrical surface: Total dimensionless local coefficient of friction is:

$$C'_F = \frac{2\tau}{\rho v_f^2} = \frac{2\nu}{\beta a v_f} \tag{VI.10}$$

Total drag on the continuous surface is:

$$D_F = 2\pi a \int_{x=0}^{x=L} \tau_f dx = \rho v_f^2 \theta \tag{VI.11}$$

The dimensionless coefficient for total drag is:

$$C_F = \frac{D}{\rho \pi a L v_f^2} = \left(\frac{\theta}{\pi a^2}\right)\left(\frac{a}{L}\right) \tag{VI.12}$$

The pumping action or total volume of the fluid entrenched by the moving surface S is:

$$q = \Delta v_f \tag{VI.13}$$

The remaining notation in the equations VI.10 through VI.13 is: θ is the momentum area in dimensionless form and may be given as

$$\frac{\theta}{\pi a^2} = \frac{e^{2\beta} - 1}{2\beta^2} - \frac{1}{\beta} - 1 \tag{VI.14}$$

where β may be defined as

$$\frac{d\beta}{dx} = \frac{4\nu}{v_f a^2} \tag{VI.15}$$

or in its integral form

$$\frac{4\nu x}{v_f a^2} = 2\int_{\beta=0}^{\beta} \left(\frac{\beta e^{2\beta} - e^{2\beta}}{\beta^2} + \frac{1}{\beta} + \frac{1}{\beta^2}\right) d\beta \tag{VI.15 a}$$

The displacement area, Δ, may be given as dimensionless displacement area

$$\frac{\Delta}{\pi a^2} = \frac{e^{2\beta} - 2\beta - 1}{2\beta} \tag{VI.16}$$

and the dimensionless boundary layer thickness, δ, is

$$\frac{\delta}{a} = e^{\beta} - 1 \tag{VI.17}$$

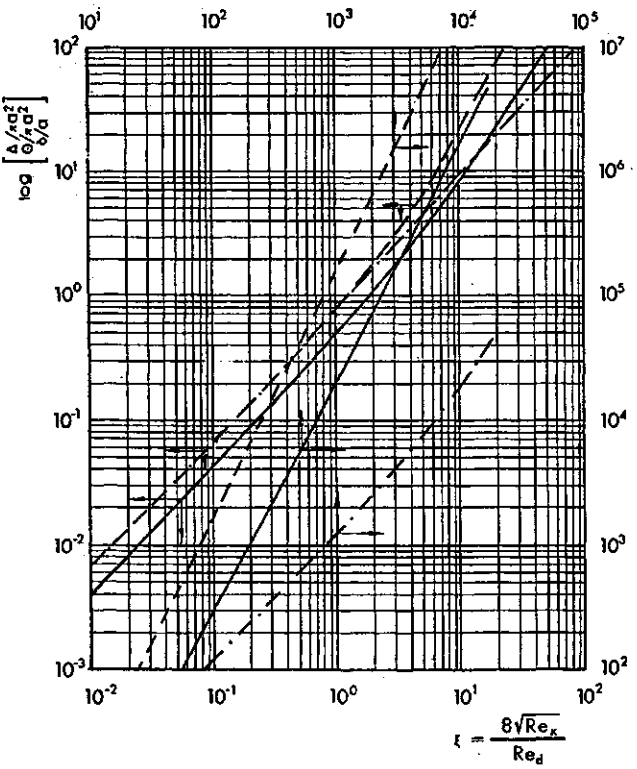

Figure VI.8: *Parameters of the moving continuous boundary layer which are dependent on ξ, a function of Reynolds numbers: δ/a – · – ; $\theta/\pi a^2$ —; $\Delta/\pi a^2$ - - -. After B. C. Sakiadis.*[3]

Figure VI.8 presents three parameters, $(\theta/\pi a^2), (\Delta/\pi a^2)$, and (δ/a) in relation to the parameter ξ, which is given by

$$\xi = 4\left(\frac{vx}{v_f a^2}\right)^{0.5} = \frac{8(Re_x)^{0.5}}{Re_d} \tag{VI.18}$$

The values of the momentum area given in the nomogram of figure VI.8 up to $\xi = 20$ may be calculated with a sufficient accuracy from the following algorithm:

$$\frac{\theta}{\pi a^2} = 1.2381\xi^{1.3428} \tag{VI.19}$$

The above quoted solution has been derived for the boundary layer problem for laminar flow, that is, for Reynolds numbers up to $Re = 10^5$. In the same series of publications, Sakiadis[3] also gives an approximate solution for turbulent flow conditions. The approach is supported by equations for continuous flat surface and determination of correcting ratios for curvature.

Total drag for turbulent flow is given as

$$D = \rho v_f^2 2\pi a\delta \left(\frac{1}{36} + \frac{1}{240}\frac{\delta}{a}\right) \tag{VI.20}$$

where δ represents the boundary layer thickness, and may be estimated from the following equation

$$\left(\frac{\delta}{a}\right)^{1.25} + 0.167\left(\frac{\delta}{a}\right)^{2.25} = 1.01\frac{x}{a}\left(\frac{v}{v_f a}\right)^{0.25} \tag{VI.21}$$

or from the formula

$$\frac{\delta}{a} = \kappa\lambda^{0.8} \tag{VI.22}$$

where

$$\lambda = \left[\frac{x}{a}\left(\frac{v}{v_f a}\right)^{0.25}\right] \tag{VI.22 a}$$

The relation between the coefficients κ and λ is given in table VI.1.

The ratio of the boundary layer thickness on a continuous cylindrical surface to the boundary layer thickness on an equivalent flat surface is

$$\frac{\delta}{\delta_p} = \kappa \tag{VI.23}$$

while the ratio of drag on the continuous cylindrical surface to the drag on an equivalent continuous flat surface is

Table VI.1
Relation between coefficients of equation for thickness of boundary layer in turbulent flow.[3]

$\lambda^{0.2}$	κ	$\lambda^{0.2}$	κ
0.0	1.000	3.0	0.281
0.5	0.987	3.5	0.220
1.0	0.891	4.0	0.177
1.5	0.682	5.0	0.122
2.0	0.500	6.0	0.088
2.5	0.671	7.0	0.068

$$\frac{D}{D_p} = \kappa\left[1 + 0.152\left(\frac{\delta}{a}\right)\right] \tag{VI.24}$$

The relationship between D/D_p and λ is given in table VI.2.

The boundary layer parameters for turbulent flow on a cylindrical surface are given also in figure VI.9. The momentum area may be calculated with good accuracy from the following simpler algorithm:

$$\log\left(\frac{\theta}{\pi a^2}\right) = -0.34256 + 1.0481\log\xi + 0.1824(\log\xi)^2 \qquad \text{(VI.25)}$$

Table VI.2
Relation between coefficients relating drag on continuous cylinder to continuous flat surface in turbulent flow.[3]

$\lambda^{0.2}$	D/D_p	$\lambda^{0.2}$	D/D_p
0.0	1.00	3.0	1.25
0.5	1.00	3.5	1.33
1.0	1.01	4.0	1.40
1.5	1.05	5.0	1.54
2.0	1.11	6.0	1.65
2.5	1.18	7.0	1.75

By Sakiadis's own admission and by later empirical investigations by many authors,[4–8] despite the apparent correctness of the theoretical solutions, the calculated coefficients of drag are much too small. Since the work by Sakiadis was published, several other attempts to solve the problems have appeared.[9–12] These works are not quoted here as the results deviate no more than 16% upwards of those of Sakiadis; it is simply not enough, by far. The general relationship used in the empirical solutions for the coefficient of drag is

$$C_f = BRe_d^a \qquad \text{(VI.26)}$$

The coefficients in equation VI.26, as quoted by different authors, are summarized in table VI.3. Measurements done by this author in a high velocity air drawing jet[15] fit fairly well with the coefficients given by Glicksman[5]; however, they fit much better with the re-evaluated results of Gould and Smith[8]. The equation coefficients for this fit are given in the last row of table VI.3. The differences quoted here amount to the calculations of Sakiadis multiplied by a factor of up to 3.5.

Gould and Smith[8] have investigated also the effect of proximity of fibers in a bundle. The authors have found that somewhere between the distance of 1200 μm and 670 μm and below, the filament boundary layers begin to affect each other to modify the drag force. For filaments spaced below that critical spacing, the coefficient of drag needs to be multiplied by a factor of approximately 0.83.

There were speculations about the reason for the deviations of the experimental coefficient of drag and the calculated values. The fluttering of the filaments, that is, vibrations of filaments along normal to the direction of motion was suggested as a potential reason. Such vibrations would change the flow pattern into

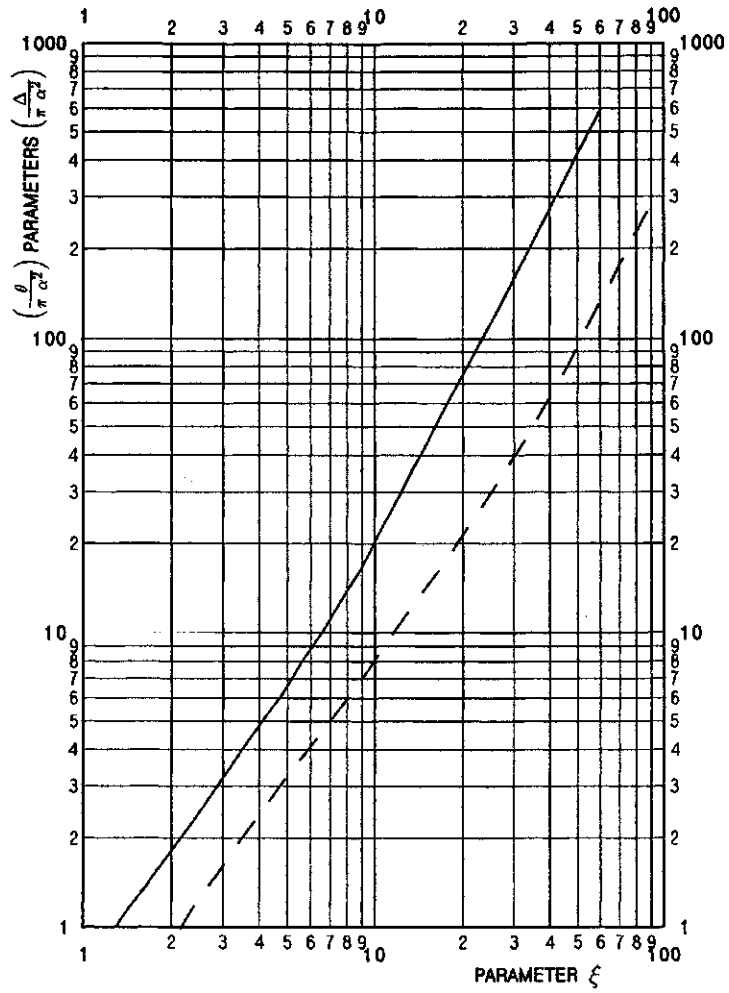

Figure VI.9: *Boundary layer parameters for cylindrical surfaces:* $\theta/(\pi a^2)$ *- continuous line,* $\Delta/(\pi a^2)$ *- dashed line. After B. C. Sakiadis*[3].

Table VI.3
Coefficients in equation VI.26 describing frictional drag.

From Re_d	To Re_d	B	a	ref
20	150	0.85	- 0.61	9
-	50	0.65	- 0.70	5
4	54	0.37	- 0.61	10
20	200	0.39	- 0.8	4
20	200	0.27	- 0.64	4, 8
20	200	0.24	- 0.61	6
50	300	0.36	- 0.50	15

a combination of axial and cross flow. Gould and Smith[8] have investigated the influence of tension applied to the filament on the drag force. They determined that freedom of movement indeed has an effect on the magnitude of drag force, and it is proportional to the fiber diameter: for filaments of 53 μm diameter, drag increased 10 %, while for 150 μm diameter, the increase amounted to 28 % at all tested velocities.

Also other interesting deviations from the boundary layer theory have been reported:[8] as the filament diameter increases above some 50 μm, the drag force decreases, eventually approaching the drag for flat plate. This area concerns filaments immediately after extrusion, close to the spinnerette, where the velocity is still small and the potential error in calculations more tolerable.

In practice, the co-current flow may be conducted close to its "pure form". Cross flow quench, the most frequently used system, always becomes a kind of "mixed flow" due to the axial flow component generated by the pumping action of the moving filaments. The flow pattern becomes even more complicated with the multifilament lines, as every row of filaments has contact with a somewhat different flow pattern of air. Solution of such problems is quoted in section VII.3.

A. Dutta[16,17] has proposed an approximate solution to estimate the magnitude of the pumping effect and its influence on uniformity of fibers in a bundle. Because of the high degree of approximation used in the solution, the work is not quoted here and the interested reader is directed to the original papers.

VI.1.c Fiber Jets

Jets[1] represent a convenient way of applying constant force drawing, provided that the fiber diameter is constant. Drawing jets are usually very forgiving for filament breaks, since a large portion of the breaks is *self threaded. Spunbond* processes use drawing jets almost as a standard of the industry. However, if substantial drawing forces are required, mechanical drawing units may be necessary, and in cases like that the jets are used to receive the fibers from the drawing rollers and to deposit them on a collecting device by simply blowing the fibers on. Naturally, there must be some kind of arrangement for an air removal on the other side of the receiving surface to prevent the fibers from being carried by the air all around.

The main body of the jets usually consists of a duct built of a sheet of metal in the form of a pipe with rectangular cross section. The smaller dimension in the circumference ranges from 10 to 25 millimeters. This "thickness" depends, obviously, on the the size of the spinline and on the questions of pressure drop, as will become clear below. The length of the main body ranges generally between 300 and 750 millimeters, only on rare occasions being longer. An example of such a jet is presented in figure VI.10.

In the design exemplified in figure VI.10, the air enters to the air tanks, which ought to be as large as a design would permit, located at both long sides of the jet. The large size of the tanks is needed to provide low velocity of air flow (assumed

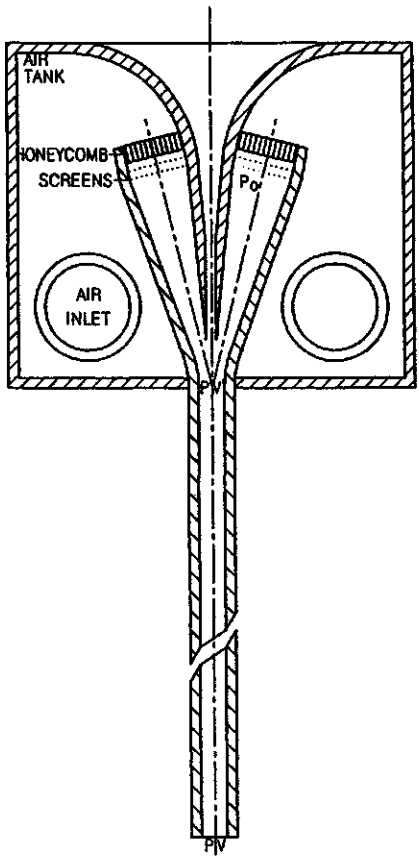

Figure VI.10: *An example of design of air jet for fiber drawing or deposition on surfaces. Explanation in text.*

zero) in this portion of the system. From the tank, the air enters through the honeycomb with a small size of cells and layer(s) of fine mesh screen(s) into a kind of short nozzle. The honeycomb and screens are to force the air into a parallel flow, to "clean" the air from possible vortices, and to create a small pressure difference between the air tank and the air entering the nozzle. Such a pressure difference helps to better equalize the air flow from the air tank to the nozzle, particularly, to equalize the air pressure along the long side of the jet.

The nozzle has a sharply decreasing cross section area to obtain highly accelerated flow. Again, this is a precaution against creation of vortices. Experience dictates that vorticity of flow is the strongest enemy of proper action of many jets, and in fact of many air machines.

At the beginning of the jet proper, the two streams of high velocity air from the two nozzles meet together with the "curtain" of fibers. From this point on the air and the fibers travel together through the length of the jet. During this travel, the air pressure becomes smaller and the air velocity increases. Since the maximum of the drag force exerted on the fibers is approximately at the beginning

of the jet, that is, at the point of junction, the velocity of fibers does not change appreciably during the travel through the jet.

Calculation of the air flow and of the jet performance must begin with a definition of the basic parameters regarding the considered number of fibers and their velocities, the force requirement, the jet design, and air flow. Here we have a number of relations to consider.

The hydraulic diameter of the jet:

$$D_h = \frac{4A}{S} \tag{VI.27}$$

where A is area of the duct cross section and S is the circumference of the duct.

The velocity of sound:

$$v_s = \sqrt{\frac{c_p}{c_v} RT} = 19.8252\sqrt{^\circ K} m/s \tag{VI.28}$$

where c_p and c_v is specific heat of air at constant pressure and constant volume, respectively; the ratio amounts to 1.4 (between $0^\circ C$ and $100^\circ C$ it changes only a fraction of one per cent). R and T have the usual meaning. The Mach number at the considered conditions is

$$M = \frac{v}{v_s} \tag{VI.29}$$

The Reynolds number for this case is defined as

$$Re = \frac{vD_h}{\mu} \tag{VI.30}$$

where μ is kinematic viscosity of air (at room temperature it is $1.4209 \cdot 10^{-2} m^2/s$).

With knowledge of the Reynolds number, one may obtain the friction factor, C_f, from the graph in figure VI.11. A more accurate value may be obtained from a numerical solution of the von Kármán - Nikuradse equation:

$$\frac{1}{\sqrt{C_f}} = -0.8 + 2log(Re\sqrt{C_f}) \tag{VI.31}$$

The other available equations of help are[18]:

$$C_f \frac{l}{D_h} = Y' - Y \tag{VI.32}$$

where

$$Y = \kappa \left\{ \frac{1}{M^2} - \left(\frac{\kappa + 1}{2} \right) \ln \left[\left(\frac{\kappa - 1}{2} \right) + \left(\frac{1}{M^2} \right) \right] \right\} \tag{VI.32 a}$$

Here Y' is Y at the entry to the jet, and $\kappa = c_p/c_v$. And another important equation is

$$\frac{p}{p'} = \frac{Z'}{Z} \tag{VI.33}$$

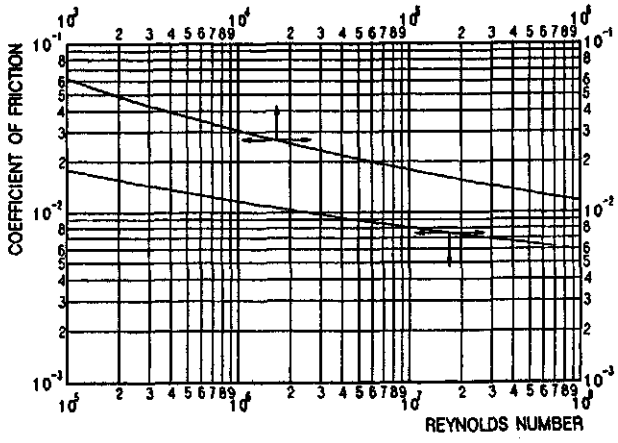

Figure VI.11: *The Kármán - Nikuradse function for friction coefficient in turbulent flow in smooth pipes. After Lukasiewicz*[18]

$$Z = M^2 \sqrt{\frac{\kappa - 1}{2} + \frac{1}{M^2}} \qquad (VI.33\,a)$$

As usually in design work, the main conceptual work is concentrated on working out the basic system in the form of a drawing. One of the biggest challenges here is a provision for the temporary widening of the fiber's entry to facilitate initial introduction of the fibers. The calculational part is rather straightforward, except it is time consuming, as all numerical solutions are.

Both, from the point of view of aerodynamics and economics, it is advantageous to design the jet so to utilize maximum of air velocity, without entering into supersonic flow. In this way, the relative velocity of air *versus* fiber will be at a maximum. The drawing force exerted on the fibers is, aside from the velocity difference, the result of fiber diameter and of the jet length. Such an approach permits the use of a minimum pressure loss due to an excessive length of the jet or large volume of air due to increase of the jet cross sectional area.

Reiterating the physical relationships one may summarize:

- The maximum of air velocity is at the exit of the jet.
- The minimum air velocity is at the beginning of the jet.
- The maximum of fiber velocity is also at the end of the jet.
- The velocity increase over the length of the jet is much larger for the air than for the fibers.
- The maximum of drawing force is located at the entry to the jet.

If the cross sectional area of the jet is small, then the friction factor is large and the air velocity gradient is very steep; the situation may arise that at the jet entry,

the fiber velocity is higher than the air velocity. Such a situation may be corrected by increasing the jet cross section, but this is connected with the requirement of larger air volume.

To impart some flexibility to the jet, and some safety margin, the velocity of air v' ought to be set higher than the fiber velocity at the entry. Based on the fiber diameter and velocity, as well as on the force requirement, one may estimate the air velocity and jet length. The equations needed for this are given in the preceeding section. It is necessary to remember that the drag force must be calculated on the velocity difference, $v_a - v_f$. The jet exit air velocity v translates into Mach number M, and its recommended value should be close to one. The pressure ratio p/p' may be read off of the table of flow parameters *versus* Mach number for subsonic flow[19] (see Appendix). The table gives also the ratio of temperature, which may be needed later to introduce corrections when working on a refinement of the initially crude calculations.

With the set velocity at the exit from the jet, it is necessary to calculate Reynolds number (equation VI.30). It is important to note that the Reynolds number so calculated is based on the maximum of air velocity, and this would lead to the largest coefficient of friction for the duct. To avoid this, the Reynolds number should be calculated on the average velocity, i.e. on the average of v' and $v = v_s$. The needed coefficient may be obtained either from figure VI.11 or from equation VI.31. However, it is better to calculate the group $C_f x/D_h$ with the help of equation VI.32. The value of Y may be treated as a constant since for $M = 1$ it amounts to $Y = 0.5580$. From the value of the group so obtained one may get the length of the duct. It often pays to prepare a graph of different lengths of jet for a range of Reynolds numbers with the "thickness" of the jet as a parameter. The width may be limited by other technological considerations.

As the next step, one may take advantage of equations VI.33. Since Z pertains to the exit conditions, $M = 1$, and furthermore Z is constant and amounts to $Z = 1.0954$. After obtaining a value for Z', one may obtain the value of p/p'. Earlier, the value of p'/p_0 was read off of the table in the Appendix. The value of p_0/p may be obtained from the relationship

$$\frac{\frac{p}{p'}}{\frac{p'}{p_0}} = \frac{p_0}{p}$$

Since $p = 1$ *ata*, p_0 is the absolute pressure needed to drive the system.

Some refinements may be introduced into the calculations after the initial results are available. Among others, it may be important to respect the temperature decrease during gas decompression. A temperature decrease of 10° to 20°C may easily take place, and this, in turn, may cause problems with room temperature or with water condensation on the equipment.

Jets like this may be operated also at lower air pressures. In such cases the performance may be obtained by somewhat different manipulation of the equations given above. Some of the solutions, particularly in cases when the sonic velocity at the exit is undesirable, may require numerical solutions of equations VI.32 and

VI.33.

A point of particular attention during such design work is that the coefficient of frictional drag decreases with increasing velocity. This is true both for the drag on fiber to be drawn, as well as for the loss of air pressure. On some occasions the decisions may be difficult to make.

It is a fair approximation that the air velocity along the jet changes linearly. Final calculation of the performance consists of the integration of the drag equation from the end of the jet where the maximum of relative velocity is found, upwards to the entry. Use of the final fiber diameter is a fair approximation.

The channel through which fibers are entering into the jet represents a point of potential air loss since there is a pressure differential on both ends. Normally the volume of lost air, Q, could be calculated as

$$Q = \frac{(p' - p)wb^3}{12\mu l} \tag{VI.34}$$

where w is the width of the channel (long dimension), b is the "thickness" of the channel, l its length, μ is, as usual, kinematic viscosity of air. However, the real situation is modified by the pumping action of the incoming fibers, and this depends on a number of factors: diameter of filaments, their number and velocity, geometry above the channel, etc. In effect, such calculations may give only orientational results.

For lay - down jets used for deposition of fibers on surfaces, the force requirement is quite low. As the removal of air underneath the collecting surface is always an unpleasant operation, minimizing the volume of air is in such cases highly recommended.

VI.2 Heat Exchange

VI.2.a Calculations

The numerous references to quench, cooling, filament temperature made throughout the preceeding chapters speak with a loud voice of the importance of temperature and heat exchange problems. The fact that the more serious work on theoretical solutions for the fiber formation have been started by E. H. Andrews[20] from calculations of temperature profile of poly(ethylene terephthalate) fibers in quench zone may be read as an additional indication of their very importance.

The heat flow equation, so familiar to engineers, is here the starting point:[20]

$$\frac{Q\rho c_p}{\pi\lambda_p}\frac{\partial T}{\partial l} = \frac{l}{u}\frac{\partial}{\partial t}\left(u\frac{\partial T}{\partial u}\right) + R^2\frac{\partial^2 T}{\partial l^2} + \frac{\partial H_F}{\partial l} \tag{VI.35}$$

The notation used here is: Q means volumetric polymer flow rate, ρ stands for polymer density, c_p is heat capacity of polymer at constant pressure, λ_p means thermal conductivity of polymer, T describes local filament temperature, l is distance from spinnerette, u is radial distance from the fiber axis, R determines the

filament radius at point l, and H_p stands for heat of phase change, which usually is crystallization.

The second term of the right hand side of equation VI.34 pertains to the conduction along the fiber axis. Since this type of heat conduction is generally considered very small in comparison with the other terms, it is therefore often omitted.

Solution of equation VI.34 is not the most easily executed task, as with all heat transfer problems. Usually a number of simplifications is introduced to make the solution more friendly. E. H. Andrews[20] separates the group

$$\frac{Q\rho c_p}{\pi\lambda_p} = Z \tag{VI.36}$$

and assumes it to be constant.† How large a variation may one assume as a constant? For example, for polypropylene from the spinnerette down to some 50° or 40°C value of Z changes by ten to fifteen per cent. In this author's opinion, for the solution of a differential equation, this is a non-negligible amount. Similar conclusions may be drawn from other publications.[21,22] Nevertheless, the same simplifications were made by many other authors.

Another source of obvious error is the generally practiced omission of heat of crystallization. Some authors apply it, but lack the information about the crystallization profile and its localization along the spinline, does falsify the results. Indeed it is difficult to say which is worse: the omission or such an incorrect application. The heat of crystallization is not a negligible quantity.

As a refinement of the work by E. H. Andrews[20], Wilhelm[23] suggests the following reasoning.

In a fiber element, at any place along the fiber traveling distance, the amount of heat delivered with the hot mass of polymer, h_1, is

$$h_1 = V dq \vartheta_{h1} \rho_p c_p \tag{VI.37}$$

and the amount of heat taken away by the mass of polymer, h_2, is

$$h_2 = V dq \vartheta_{h2} \rho_p c_p \tag{VI.38}$$

where h is the amount of heat, V is local filament velocity, q means filament cross section, ϑ stands for local filament temperature, ρ_p means density of polymer, and c_p describes specific heat of the polymer at constant pressure.

Besides the convective heat transfer, there also exists a heat transfer which, according to Fourier's equation, is

$$h_2 = \lambda_p \nabla^2 dQ \tag{VI.39}$$

where λ describes thermal conductivity of polymer, and Q represents volumetric polymer flow rate.

†Data on certain physical properties and their functions of temperature for some polymers are given in the Appendix.

The heat balance for a polymer segment is

$$h_1 - h_2 = h_3 \tag{VI.40}$$

and further

$$V dq(\vartheta_{q1} - \vartheta_{q2})\rho_p c_p = \lambda_p \nabla^2 \vartheta dQ \tag{VI.41}$$

Fiber velocity V may be represented as dl/dt, where l is distance along the fiber axis, and t is time. The change of temperature $(\vartheta_{q1} - \vartheta_{q2})$ may be written as $d\vartheta$. The physical properties of the polymer may be accumulated into a temperature conductivity number

$$a_p = \frac{\lambda_p}{c_p \rho_p} \tag{VI.42}$$

which permits us to rewrite equation VI.41 as

$$\frac{dl dq}{dt} d\vartheta = a_p \nabla^2 \vartheta dQ \tag{VI.43}$$

Since $dq \cdot dl = dQ$ equation VI.43 obtains a form

$$\frac{d\vartheta}{dt} = a_p \frac{\partial^2 \vartheta}{\partial u^2} + \frac{1}{u}\frac{\partial \vartheta}{\partial u} + \frac{\partial^2 \vartheta}{\partial l^2} \tag{VI.44}$$

where u continues to mean the radial distance from the fiber axis.

From the continuity equation we have

$$V = \frac{dl}{dt} = \frac{Q}{\pi R^2} \tag{VI.45}$$

so equation VI.45 may obtain the following form

$$\frac{\partial \vartheta}{\partial l}\frac{Q c_p \rho_p}{\pi \lambda_p} = R^2 \frac{\partial^2 \vartheta}{\partial u^2} + \frac{R^2}{r}\frac{\partial \vartheta}{\partial u} + R^2 \frac{\partial^2 \vartheta}{\partial l^2} \tag{VI.46}$$

The second group on the left hand side of equation VI.44 is equal to Z, as it was defined in equation VI.36.

In further steps Andrews makes somewhat strange assumptions and simplifications with a loss of accuracy. The equation was solved by E. L. Albasiny[24] numerically using nondimensional variables in a way which appears more satisfactory and accurate. And so, temperature ϑ is changed to nondimensional form by division with initial melt (spinnerette) temperature, T_0

$$\theta = \frac{\vartheta}{T_0} \tag{VI.47}$$

and by dividing the radial position, u, by the filament radius at a given distance from spinnerette

$$r = \frac{u}{R} \tag{VI.48}$$

Further, instead of distance, l, time, t is used. The last change is a matter of choice, it may depend on which form the function F, which describes the heat loss from the filament surface or the surface temperature, is available. Following Wilhelm[23], the change (loss) of heat may be defined as

$$dh = \alpha\theta dq \tag{VI.49}$$

where the surface segment $dq = 2\pi R dl$ and α is the heat transfer coefficient. From Fourier's formula

$$dh = -\lambda_p \frac{\partial\theta}{R\partial r} dq \Big|_{r=1} \tag{VI.50}$$

Equations VI.49 and VI.50 give the spatial boundary condition

$$\frac{\alpha R}{\lambda_p} = \frac{1}{\theta}\frac{\partial\theta}{\partial r}\Big|_{r=1} \tag{VI.51}$$

The heat transfer coefficient, α, may be substituted with an empirical function of heat loss from the filament surface, F, per unit length per time and degree of temperature.

$$-\frac{F(l)}{2\pi\lambda_p} = \frac{r}{\theta}\frac{\partial\theta}{\partial r}\Big|_{r=1} \tag{VI.51 a}$$

Further, boundary conditions are set as

$$\theta = 1 \quad \text{for all} \quad r \quad \text{at} \quad t = 0 \tag{VI.52}$$

$$\frac{\partial\theta}{\partial r} \quad \text{at} \quad r = 0 \tag{VI.53}$$

$$\frac{1}{\theta}\frac{\partial\theta}{\partial r} = -F(t) \quad \text{at} \quad r = 1 \tag{VI.54}$$

Now equation VI.46 becomes

$$Z\frac{\partial\theta}{\partial t} = \frac{\partial^2\theta}{\partial r^2} + \frac{1}{r}\frac{\partial\theta}{\partial r} \tag{VI.55}$$

for $0 < r < 1$. As it was mentioned above, the term describing heat conduction in the axial direction is omitted as insignificantly small.

Albasiny[24] applies the Crank-Nicolson[25] method for the finite difference approximation because of its good stability within the wide range of intervals used. Denoting as θ_i, Φ_1, and ϕ the values of $\theta(t)$, $\theta(t+\delta t/2)$, and $\theta(t+\delta t)$, respectively at the points $r_i = i\delta r$, where $i = 0, 1, 2, 3, ..., n$ and $\delta r = 1/n$, the finite difference representation of equation VI.54 becomes

$$Z\frac{\phi_1 - \theta_1}{\delta t} = \frac{1}{2(\delta r)^2}\left\{\phi_{i+1} - 2\phi_i + \frac{\phi_{i+1} - \phi_{i-1}}{2i} + \theta_{i+1} - 2\theta_i + \theta_{i-1} + \right.$$
$$\left. + \frac{\theta_{i+1} - \theta_{i-1}}{2i} - C_i(\phi_i) - C_i(\theta_i)\right\} + \frac{Z}{\delta t}C_t(\Phi_t) \tag{VI.56}$$

Here all the values C represent "difference corrections". For approximate calculations they may be neglected, but for accurate calculations they ought to be respected. $C_i(\phi_i)$ and $C_i(\theta_i)$ may be expressed in terms of differences in the r-direction. The correction $C_t(\Phi_t)$, however is connected to the differences in the time (or distance, as the case may be) direction. This term may be calculated, but the task is hard even for a computer; it may be made negligible if the interval δt is very small. This way is usually selected. According to the standard central difference notation, as given by Crank and Nicolson[25], the initial terms for the corrections are

$$C_i(\theta_t) = \frac{1}{6i}\mu\delta_r^3\theta_i + \frac{1}{12}\delta_r^4\theta_i + \doteq \tag{VI.57}$$

$$C_t(\Phi_i) = -\frac{1}{12}\delta_t^3\Phi_i + \frac{1}{120}\delta_t^5\Phi_i + \doteq \tag{VI.57 a}$$

The subscripts r and t indicate the difference operation in the r- or t-direction, respectively. μ represents the eigenvalue of the matrix representing the set of equations.

When starting the calculations from $t = 0$ (or $l = 0$), all the values from $\theta_0, \theta_1, ..., \theta_n$ are known. In such a case, equation VI.56 with $i = 1, 2, ..., n-1$ gives a set of $n-1$ simultaneous equations for $n+1$ unknowns $\phi_0, \phi_1, ..., \phi_n$. The two additional equations may be obtained when using VI.56 with $i = 0$ and $i = n$, but this way we introduce two additional unknowns ϕ_{-1} and ϕ_{n+1}. However, the boundary conditions VI.52 and VI.53 permit the elimination of those two additional unknowns, as at $i = 0$ the condition $\partial\theta/\partial r = 0$, which results from the symmetry condition

$$\theta_{-1} = \theta_{+1} \qquad \phi_{-1} = \phi_{+1} \tag{VI.58}$$

The term $(1\theta)\partial\theta/\partial r$ is replaced by its limiting value $\partial^2\theta/\partial r^2$. The condition $(1\theta)\partial\theta/\partial r = -F(t)$ at $i = n$ may be represented by the following

$$\frac{\theta_{n+1} - \theta_{n-1}}{2\delta r} - \frac{1}{6\delta r}\mu\delta^3\theta_n + ... = -\theta_n F(t) \tag{VI.59}$$

$$\frac{\phi_{n+1} - \phi_{n-1}}{2\delta r} - \frac{1}{6\delta r}\mu\delta^3\phi_n + ... = -\phi_n F(t+\delta t) \tag{VI.59 a}$$

Equations VI.56 and VI.59 may be combined and written in the following, operationally useful, way

$$p_i\phi_{i+1} - s\phi_i + (2-p_i)\phi_{i-1} = -p_i\theta_{i+1} + m_i\theta_i - (2-p_i)\theta_{i-1} + C_i(\phi_i) + C_i(\Theta_i) \tag{VI.60}$$

for $i = 0, 1, 2, ..., n$ where

$$p_0 = 2 \tag{VI.61}$$

$$s_0 = 2 + Z\frac{(\delta r)^2}{\delta t} \tag{VI.61 a}$$

$$m_0 = 2 - Z\frac{(\delta r)^2}{\delta t} \tag{VI.61 b}$$

$$C_0(\theta_0) = \frac{1}{12}\delta^4\theta_0 + ... \qquad (VI.61\,c)$$

$$p_i = 1 + \frac{1}{2i} \qquad (VI.62)$$

$$s_i = 2\left[1 + Z\frac{(\delta r)^2}{\delta t}\right] \qquad (VI.62\,a)$$

$$m_i = 2\left[1 - Z\frac{(\delta r)^2}{\delta t}\right] \qquad (VI.62\,b)$$

$$C_i(\theta_i) = \frac{1}{6i}\mu\delta^3\theta_i + \frac{1}{12}\delta^4\theta_i + ... \qquad (VI.62\,c)$$

$$p_n = 0 \qquad (VI.63)$$

$$s_n = 2\left[1 + Z\frac{(\delta r)^2}{\delta t}\right]2\left(1 + \frac{\delta r}{2}\right)\delta r F(t + \delta t) \qquad (VI.63\,a)$$

$$m_n = 2\left[1 - Z\frac{(\delta r)^2}{\delta t}\right]2\left(1 + \frac{\delta r}{2}\right)\delta r F(t) \qquad (VI.63\,b)$$

$$C_n(\theta_n) = \frac{1}{3}\mu\delta^3\theta_n + \frac{1}{12}\delta^4\theta_n + ... \qquad (VI.63\,c)$$

Solution of equation VI.59 requires solution of a set of $n+1$ equations at each step of the unknown ϕ_i. In matrix notation the problem may be given as

$$\mathbf{A}\theta(t + \delta t) = \mathbf{B}\theta(t) \qquad (VI.64)$$

where $\mathbf{A}$ and $\mathbf{B}$ are square matrices of order $n+1$ independent of t (or l). $\theta(t)$. $\theta(t)$ and $\theta(t + \delta t)$ are column vectors with components θ_i and ϕ_i, respectively. At time $j\delta t$ is

$$\theta(j\delta t) = (\mathbf{A}^{-1}\mathbf{B})^j\theta(0) \qquad (VI.65)$$

If the matrix $\mathbf{A}^{-1}\mathbf{B}$ has eigenvalues λ_i and eigenvectors $\mathbf{v}_i$, one may write

$$\theta(0) = \sum_{i=0}^{n} c_i\mathbf{v}_i \qquad (VI.66)$$

where c_i are constants. In effect, equation VI.65 may be rewritten as

$$\theta(j\delta t) = \sum_{i=0}^{n} c_i\lambda_i^j v_i \qquad (VI.67)$$

If we denote $Z(\delta r)^2/\delta t = b$ then

$$\mathbf{A} = -(\mathbf{C} + 2b\mathbf{I}) \qquad (VI.68)$$

$$\mathbf{A} = \mathbf{C} - 2b\mathbf{I} \qquad (VI.68\,a)$$

where $\mathbf{I}$ is the identity matrix of order $n+1$ and $\mathbf{C}$ is the square matrix of order $n+1$ given as

$$\mathbf{C} = \begin{vmatrix} 4 & -4 & . & . & . & . & . \\ -.5 & 2 & -1.5 & . & . & . & . \\ . & . & . & . & . & . & . \\ . & . & -(1-\frac{1}{2i}) & 2 & -(1+\frac{1}{2i}) & . & . \\ . & . & . & . & . & . & . \\ . & . & . & . & -\{1-\frac{1}{2n-2}\} & 2 & -\{1+\frac{1}{2n-2}\} \\ . & . & . & . & -2 & 2 & 2\delta r\{1+\frac{\delta r}{2}\} \end{vmatrix} \tag{VI.69}$$

It needs to be pointed out that $\mathbf{C}$ is independent of δt. The eigenvalues, λ_i, and eigenvectors, $\mathbf{v_i}$ are defined through the following two equations.

$$(\mathbf{A}^{-1}\mathbf{B} - \lambda_i \mathbf{I})\mathbf{v}_i = 0 \tag{VI.70}$$

$$(\mathbf{B} - \lambda_i \mathbf{A})\mathbf{v}_i = 0 \tag{VI.71}$$

When taking advantage of the equations VI.68, one obtains

$$\left\{\mathbf{C} - \frac{2b(1-\lambda_i)}{(1+\lambda_i)} \cdot \mathbf{I}\right\}\mathbf{v}_i = 0 \tag{VI.72}$$

This shows that vectors $\mathbf{v}_i$ are eigenvectors of $\mathbf{C}$ and the eigenvalues λ_i are related to the eigenvalues, μ_i of $\mathbf{C}$ through the following equations.

$$\mu_i = \frac{2b(1-\lambda_i)}{(1+\lambda_i)} \tag{VI.73}$$

$$\lambda_i = \frac{2b-\mu_i}{2b+\mu_i} \tag{VI.73 a}$$

The time dependence of the solution is realized through equations VI.73 since the value of the group b depends on δt. As the stability criterion, Albasiny[24] gives the following set of requirements.

$$|\lambda_i| < 0 \qquad \text{and} \qquad |\lambda_0| > |\lambda_n|$$

This leads to the restriction on the choice of values of δt for any assumed values of n.

$$b > \frac{\sqrt{\mu_0 \mu_n}}{2} \tag{VI.74}$$

$$\delta t < \frac{2Z}{n^2\sqrt{\mu_0 \mu_n}} \tag{VI.74 a}$$

When applying the difference correction, equation VI.64 must be replaced with the following formulation

$$(\mathbf{A} + \mathbf{D})\theta(t+\delta t) = (\mathbf{B} - \mathbf{D})\theta(t) \tag{VI.75}$$

where **D** is a matrix from the difference corrections. It is assumed that the corrections of order higher than fourth may be easily neglected. To compute the correction $C_i(\theta_i)$ for $i = 0, 1, n-1$, and n, it is necessary to know the values of $\theta_{-2}, \theta_{-1}, \theta_{n+1}$, and θ_{n+2}, it is the values outside of the normal course of calculations. From the symmetry criterion it follows that $\theta_{-2} = \theta_2$ and $\theta_{-1} = \theta_1$. The remaining values may be obtained from the extrapolation formula:

$$\theta_{i+1} = 6\theta_i - 15\theta_{i-1} + 20\theta_{i-2} - 15\theta_{i-3} + 5\theta_{i-4} - \theta_{i-5} \qquad \text{(VI.76)}$$

for $i = n, n+1$. In all the equations from VI.64 to VI.73, the matrix **C** needs to be replaced with **C** − **D**, if the corrections are to be applied.

Naturally, other ways of solving the problem of heat transfer within a fiber may also be used, as will be shown below. Nonetheless, the combined method of Andrews,[20] - Wilhelm[23] - Albasiny[24] proves to be very reliable, relatively simple and easily handled by desk computers. The size of δt or δl, as the case may be, resulting from the stability criteria may well be reduced. Much improved results may be obtained if the Z-value is constantly updated to the actual temperature, and numerical calculations lend themselves easily to such an operation. However, correct results may only be obtained with application of the heat of crystallization generated during the process.

If a "crystallization history" (as given in section IV.5) is obtained it may easily be synchronized with the temperature being calculated. The amount of polymer crystallized may be calculated for each radial position. From the heat of crystallization and specific heat, as appropriate due to the temperature at any given point, the temperature increase may be calculated. Such a correction must be added to every appropriate temperature before moving further by the next increment in time. An example of results of such calculations may be seen in figures VI.12, VI.13, and VI.14, VI.15.

The calculations described by figures VI.12 and VI.13 were performed on the basis of measured fiber diameter and surface temperature. Results for a number of processes carried out on different machines and under different conditions were used to determine heat transfer coefficient due to convection. Heat losses due to radiation were calculated separately according to Stefan-Boltzmann law, which in adaptation to the fiber shape gives the following equation.

$$H_{rad}(l) = 2\varepsilon\sigma\sqrt{\pi Q} \times \left(\frac{T_s^4 - T_a^4}{T_s - T_a}\right) \qquad \text{(VI.77)}$$

where ε is emissivity, σ represents the Stefan- Boltzmann constant $= 5.6687 \cdot 10_{-12} J/(cm^2 s^{2\circ} K^4)$, T_s and T_a, temperatures of fiber surface and surrounding, respectively in $^\circ K$.

Nusselt number was calculated on the basis of the experimental data. The processes studied were fast and the fast moving threadline had considerable pumping action. The pumping action in conjunction with a cross flow quench calls for the consideration of the use of two separate air velocities. An exception is several centimeters below the spinnerette, where the cross flow component is practically

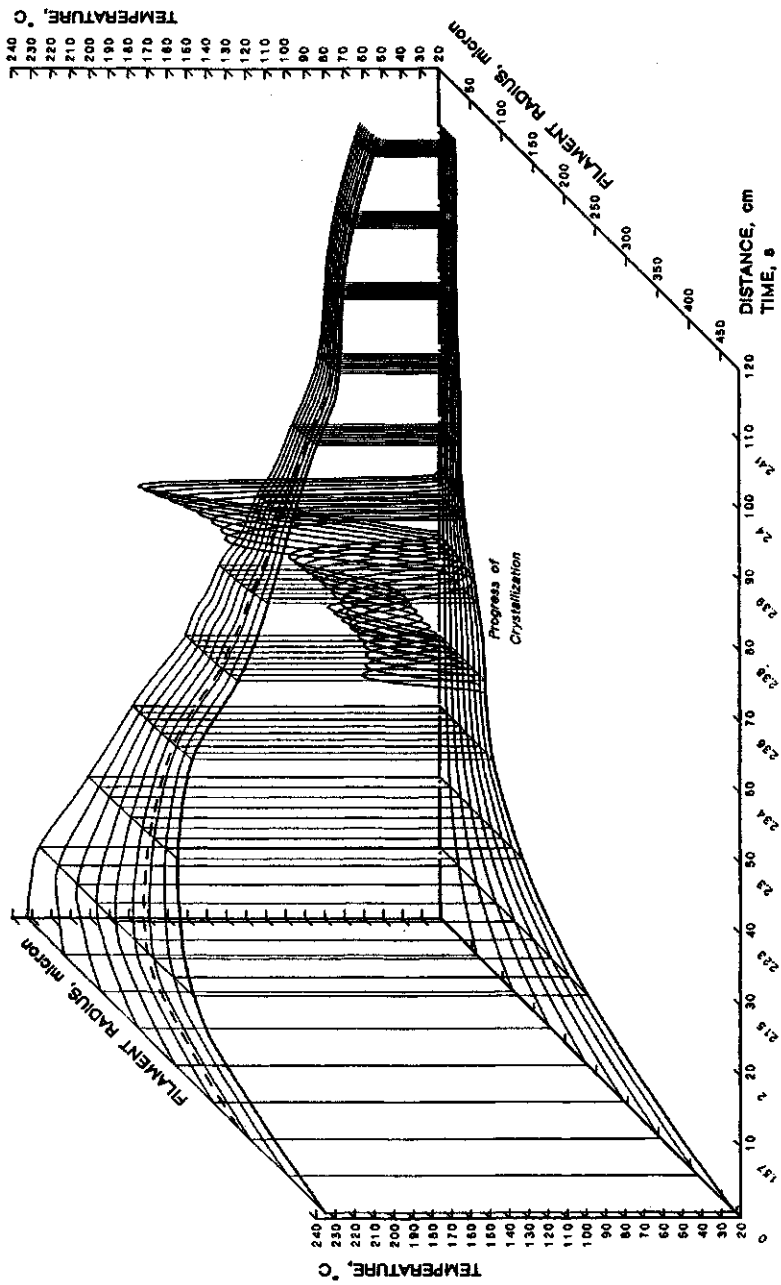

Figure VI.12: *Mapping of temperature, diameter, and crystallization rate changes against distance in formation of fibers from polypropylene, medium fast process.*

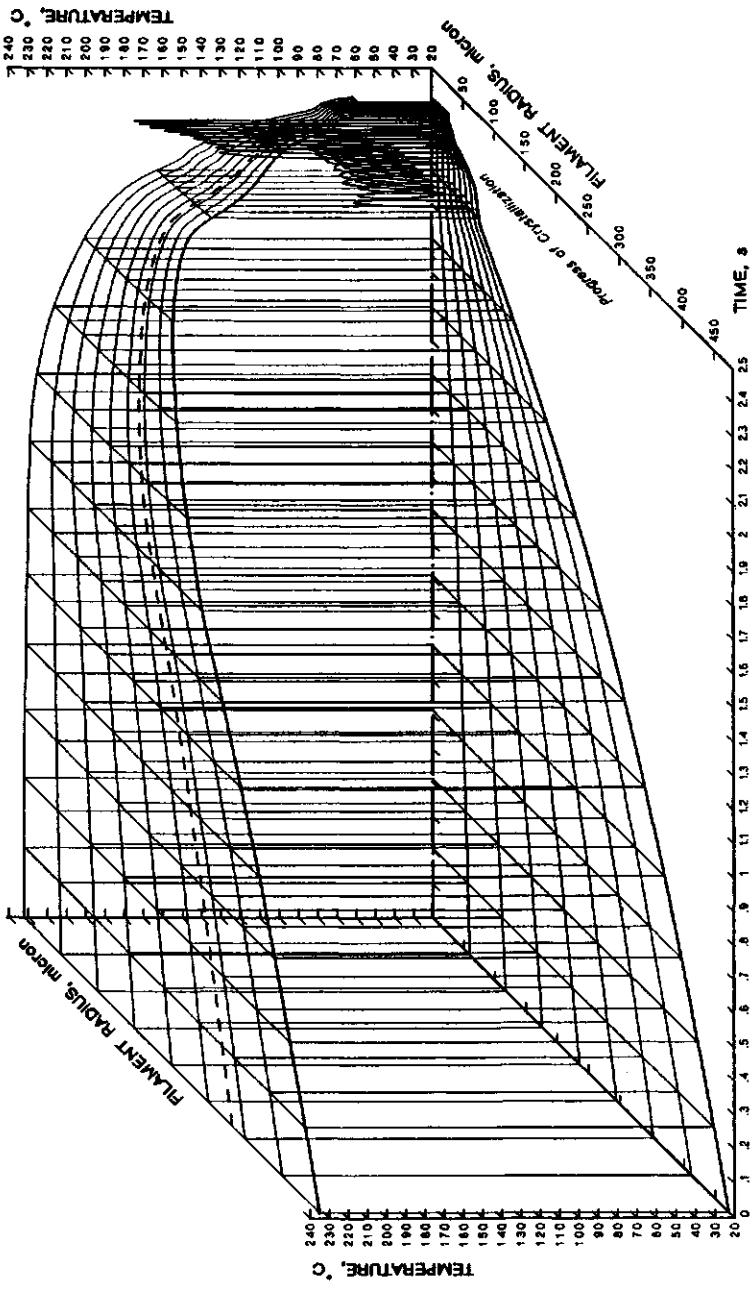

Figure VI.13: *The same process as in figure VI.12, except the mapping is against time.*

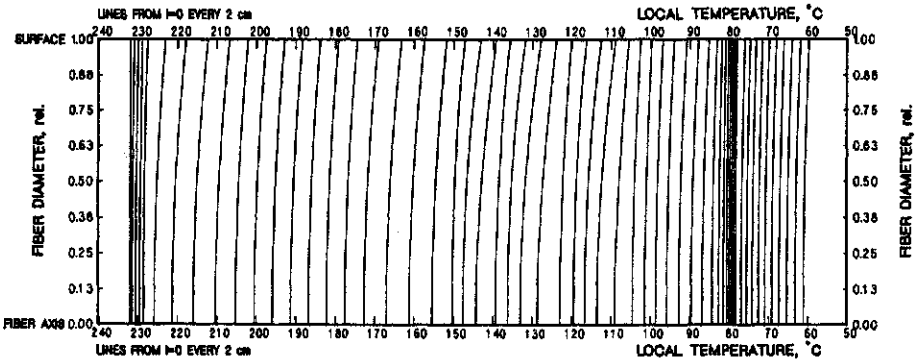

Figure VI.14: *Plot of temperature against fiber radius with 2cm intervals along the formation path. The same process as in figures VI.12 and VI.13.*

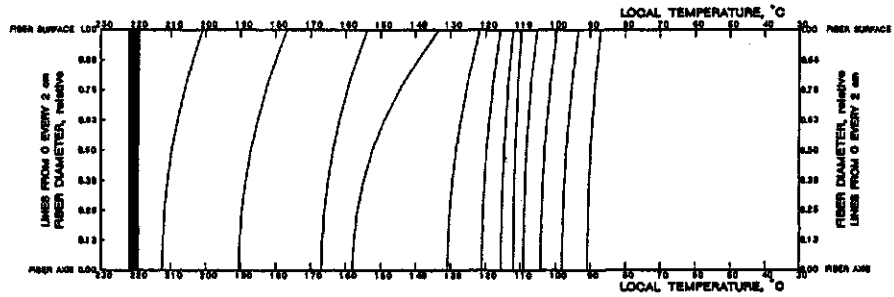

Figure VI.15: *Plot of temperature against fiber radius with 2cm intervals along the formation path. Polypropylene fiber formation with extremely intensive quench, medium fast process.*

equal zero. And so, one Reynolds number, Re_l, was calculated on the basis of the length from spinnerette, as in Sakiadis's calculations. The other Reynolds number, Re_d, was calculated on the fiber diameter and the cross flow air component. The air velocities and air temperature were mapped in the vicinity of the threadline and gave basis for the calculations.

The definition of Nusselt number is:

$$Nu = \frac{\alpha d}{\lambda_a} \tag{VI.78}$$

α is coefficient of heat transfer, λ_a is heat conductivity of air, v_f is fiber velocity, d is fiber diameter, c_{pa} is heat capacity of air at constant pressure, η_a is dynamic viscosity of air.

For $Re_l < 20$

$$Nu = 0.3298 + .015893 Re_l \tag{VI.79}$$

For $Re_d < 5.0$ and $Re_l \times Re_d < 150$

$$Nu = 0.2151 Re_l^{0.3003} \exp(0.5612 Re_d) \qquad (VI.79\,a)$$

For $Re_d < 5.0$ and $150 \leq Re_l \times Re_d \leq 6000$

$$Nu = 0.5110 Re_l^{0.1837} \exp(0.1258 Re_d) \qquad (VI.79\,b)$$

For $Re_d < 5.0$ and $Re_l \times Re_d \leq 10000$

$$Nu = 3.2745 Re_l^{-0.03844} Re_d^{0.2365} \qquad (VI.79\,c)$$

For $Re_l \times Re_d > 10000$

$$Nu \approx 3.55 \text{ to } 3.75 \qquad (VI.79\,d)$$

One must allow a suspicion that in the experiments which permitted calculation of equations VI.79, the changes of Reynolds numbers formed some kind of a pattern of mutual interrelationships. For this reason equation VI.79 is not to be taken as an "iron" rule, it is rather an indication of a dependence of the boundary layer on the actual geometry of flow, and, in consequence, on the character of heat exchange. The problem of air flow as it interacts with the motion of filaments requires a broad and systematic investigation. It is acutely necessary for calculation of heat transfer, as well as for the design of flow patterns for the quench air.

The heat transfer equation (VI.46) may be solved with the help of Bessel functions.[20,23,24] After grouping of the "constants" into Z (equation VI.36), further substitution is made:[20]

$$\theta(l,r) \equiv S(l,r)\tau(l) \qquad (VI.80)$$

As a result equation VI.46 becomes

$$\frac{Z}{\tau}\frac{\partial \tau}{\partial l} = \frac{1}{S}\left(\frac{1}{r}\frac{\partial S}{\partial r} - Z\frac{\partial S}{\partial l} + \frac{\partial^2 S}{\partial r^2}\right) \qquad (VI.81)$$

Both sides of this equation have been taken to be equal to $-p^2$, which is a function of l only.

$$\frac{Z}{\tau}\frac{\partial \tau}{\partial l} = -p^2(l) \qquad (VI.82)$$

$$\tau(l) = a \exp\left(-\int_0^1 \frac{p^2}{Z} dl\right) \qquad (VI.83)$$

And in effect

$$\frac{\partial^2 S}{\partial r^2} + \frac{1}{r}\frac{\partial S}{\partial r} + S\left(p^2 - \frac{Z}{S}\frac{partial S}{\partial l}\right) = 0 \qquad (VI.84)$$

Further, Andrews assumes that

$$\frac{Z}{S}\frac{\partial S}{\partial l} \ll p^2 \qquad (VI.85)$$

and in this way equation VI.84 becomes Bessel's equation of zero order with the general approximate solution

$$\theta(l,p,r) = B(l)J_0(p,r) \times \exp\left(-\int_0^1 \frac{p^2}{Z}dl\right) \tag{VI.86}$$

where $B(l)$ is an integration constant depending on the boundary conditions, $J_0(p,r)$ is Bessel's function of zero order of the form

$$J_0(p,r) = 1 - \frac{(pr/2)^2}{(1!)^2} + \frac{(pr/2)^4}{(2!)^2 3} - frac(pr/2)^6(3!)^2 4 + \ldots - \ldots \tag{VI.87}$$

By combining equation VI.87 with the radial boundary conditions given by equation VI.51a we have

$$\frac{1}{m} = \frac{F(l)}{2\pi\lambda_p} = p\frac{J_1(p)}{J_0(p)} \tag{VI.88}$$

where J_1 is Bessel's function of first order of the form

$$J_1(p,r) = \frac{pr}{2}\left[1 - \frac{(pr/2)^2}{(1!)^2} + \frac{(pr/2)^4}{(2!)^2 3} - \frac{(pr/2)^6}{(3!)^2 4} + \ldots - \ldots\right] \tag{VI.89}$$

Equation VI.88 has an infinite number of solutions p'_j for each value of $F(l)$. Andrews applies a correction for the p'_j values.

$$p_j^2 = p_j'^2 - \psi \tag{VI.90}$$

where the correction coefficient equals

$$\psi = \frac{Z}{BJ_0}\frac{\Delta BJ_0}{\Delta l} \tag{VI.91}$$

This correction is the result of the approximation defined by equation VI.85. The differences are calculated from the values for the beginning and the end of the considered section of the threadline.

The boundary conditions that $\theta = \theta_0$ for all values of r at $l = 0$ (equation VI.52) give

$$B_j = \frac{2\theta_0}{p_j}\frac{J_1(p_j)}{J_0^2(p_j) + J_1^2(p_j)} \tag{VI.92}$$

Finally for the cooling of a filament one obtains

$$\theta(l,r) = 2\theta_0 \times \sum_{j=0}^{\infty} \frac{J_1(p_j)J_0(p_j r)}{p_j[J_0^2(p_j)J_1^2(p_j)]} \times \exp\left\{-\int_0^1 \frac{p_j^3}{Z}dl\right\} \tag{VI.93}$$

Shimizu and co-workers[26] have studied heat transfer in formation of polypropylene filaments. Among others, the authors published very instructive results of measurements of the air temperature around the filament. These results are

given in figure VI.16. The thickness of the envelope increases with increasing intensity of polymer flow, and it decreases with the flow intensity of cooling air, as it is easy to predict. The relatively large diameter of the envelope of hot air must be vulnerable to distortion by both laminar flow of the cooling air, as well as, or even more so, to a turbulent flow and vorticity. This appears to be a good explanation of the fact that there were so many and so different correlations of Nusselt number published, and that the results are so widely scattered, even for relatively similar flow conditions.[55] It is to be expected that for more drastic conditions, typical of commercial operations, the discrepancies for the Nusselt number may be even larger.

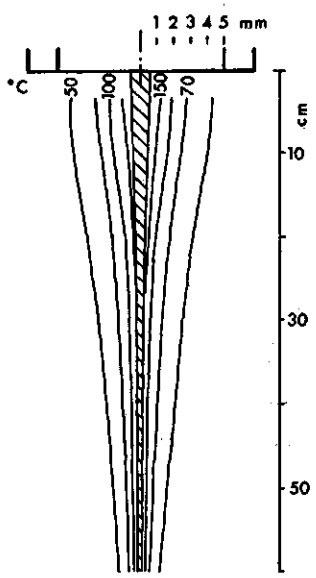

Figure VI.16: *Air temperature distribution around a melt spun filament. Melt temperature of 258 °C, take-up velocity 0.56m/s. Reproduced after J. Shimizu & al.*[26]

It is for these reasons why experience dictates that for the serious work of defining the formation conditions, it is substantially more accurate to measure the filament surface temperature rather than calculate it from the air flow data. Air flow and temperature measurements in the vicinity of a running filament are much less accurate than filament surface measurements. In addition, the calculated heat transfer coefficient may be also less certain.

Because of similar reasons, use of the numerical calculations is preferred over the method based on use of Bessel's function. The numerical calculations, besides having a little edge on the accuracy, seem to alow more flexibility, particularly if complex calculations of the entire process description are conducted. A much more accurate method has been suggested by T. Matsui and S. Kase.[27,28] These authors suggest calculation of temperature distribution across the plane of a fiber cross section, not just across a radius. There are no experimental techniques

available for exact corroboration of the results of such calculations; nevertheless, the method is of importance for research purposes, especially with cross flow, or otherwise asymmetrical, quench.

Matsui and Kase[27,28] assume an equivalence between the steady state heat conduction within a filament being formed and a stationary circular disk of fixed diameter. The asymmetry was introduced into the computations by use of non-symmetric data on Nusselt number which are the result of the air flow around a circular cylinder (see section VI.1.b and figure VI.4) and calculated by Eckert and Soehungen.[29]

The authors assume:

- steady state formation
- constant polymer density, ρ
- axisymmetric and purely extensional flow of polymer
- negligible viscous heat formation and dissipation
- negligible heat conduction in the axial direction.

As a result of the assumptions Matsuo and Kase begin with the following equations for continuity and energy, respectively. The equations are formulated in the cylindrical coordinate system, as shown in figure VI.17.

$$\frac{1}{r}\frac{\partial}{\partial r}(rv_r) + \frac{\partial v}{\partial x} = 0 \tag{VI.94}$$

$$\rho C_p \left(v_r \frac{\partial T}{\partial r} + v\frac{\partial T}{\partial x}\right) = \lambda \left[\frac{1}{r}\frac{\partial}{\partial r}\left(r\frac{\partial T}{\partial r}\right) + \frac{1}{r^2}\frac{\partial^2 T}{\partial \beta^2}\right] \tag{VI.95}$$

where T is temperature, v is velocity in the x direction, C_p is specific heat of polymer, and λ is heat conductivity of polymer.

The profile of change of filament radius is input into the calculations; the authors used a computed profile, but an experimental profile may be used as well.

In a purely extensional flow, axial velocity is independent of the radius and therefore equation VI.94 may be written as

$$v_r = -\frac{r}{2}\frac{dv}{dx} \tag{VI.96}$$

and this shows that radial velocity, v_r, is directly proportional to the radial coordinate r. The streamline in figure VI.18 may be described by

$$\frac{dr}{dx} = \frac{v_r}{v} = -\frac{r}{2v}\frac{dv}{dx} \tag{VI.97}$$

On integration, equation VI.97 yields $\pi r^2 v = const.$ = volume flow rate within radius r, and further for the filament radius R it follows that $\pi R^2 v = const. = Q$,

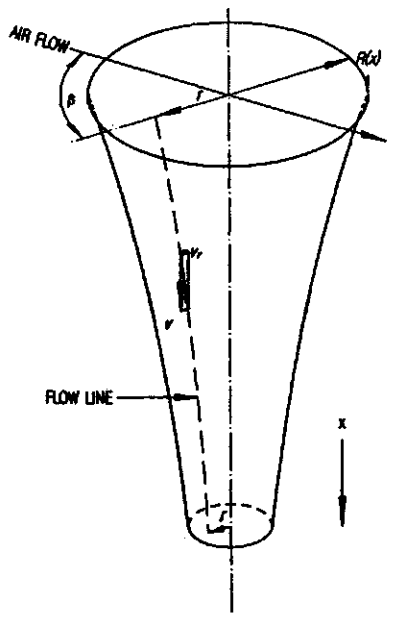

Figure VI.17: *Schematic representation of the heat conduction by T. Matsuo and S. Kase.*[27,28]

i.e. total flow rate. In view of the above, a streamline is uniquely identified by p and β, where

$$p = \frac{r}{R(x)} \tag{VI.98}$$

and β is the angle, in this case the angle with the direction of air flow.

If one assumes a filament (figure VI.18) as a stack of infinitely thin discs, than a point on a disc may be identified by its corresponding streamline and time, τ, or by three parameters p, β, and τ. In this way, in equation VI.95 the variable of length x is converted into time, τ, and

$$\tau = \int_0^x \frac{dx}{v(x)} \tag{VI.99}$$

Differentiation of temperature with respect to time along a streamline, with $p = const.$ gives

$$\left(\frac{\partial T}{\partial \tau}\right)_{p=const} = \frac{\partial T}{\partial x}\frac{dx}{d\tau} + \frac{\partial T}{\partial r}\left(\frac{\partial r}{\partial \tau}\right)_{p=const.} = \frac{\partial T}{\partial x}v + \frac{\partial T}{\partial r}v_r \tag{VI.100}$$

If we substitute equation VI.100 into the left hand side of equation VI.95, and equation VI.98 into the right hand side, we have

$$\frac{R^2\rho C_p}{\lambda}\left(\frac{\partial T}{\partial \tau}\right)_{p=const.} = \frac{1}{p}\frac{\partial}{\partial p}\left(p\frac{\partial T}{\partial p}\right) + \frac{1}{p^2}\frac{\partial^2}{\partial \beta^2} \tag{VI.101}$$

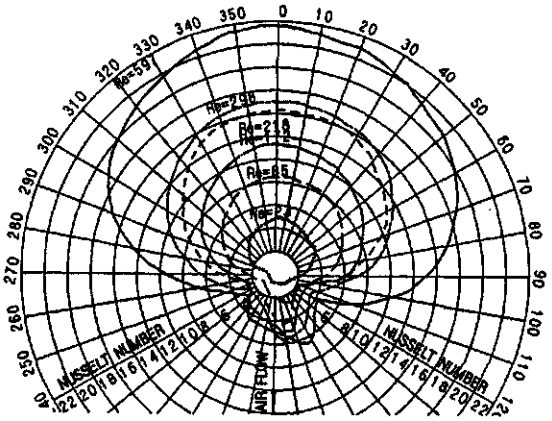

Figure VI.18: *Nusselt number around a stationary cylinder cooled by air flowing perpendicularly. After E. R. G. Eckert and E. Soehungen*[29]

Substitution of equation VI.99 onto VI.101 yields

$$\frac{R^2\rho C_p}{\lambda}\frac{\partial T}{\partial \tau} = \frac{R^2\rho C_p}{\lambda} v \frac{\partial T}{\partial x} \tag{VI.102}$$

Here the restriction of $p = const.$ for $\partial T/\partial x$ is implied.

Since $R^2 v = const.$, a new variable, X is created

$$X = \frac{\lambda x}{\rho C_p v R^2} = \frac{\pi \lambda}{Q_m C_p} \tag{VI.103}$$

where Q_m is polymer mass flow. With the new variable, X, equation VI.101 becomes

$$\frac{\partial T}{\partial X} = \frac{1}{p}\frac{\partial T}{\partial p} + \frac{\partial^2 T}{\partial p^2} + \frac{1}{p^2}\frac{\partial^2 T}{\partial \beta^2} \tag{VI.104}$$

Equation VI.104 represents unsteady two dimensional heat conduction with a ficticious time variable X. In this way, this is a two dimensional transient heat conduction within a disc of radius p.

The boundary conditions for Matsuo and Kase's solution have been set as follows:

At the filament surface

$$\lambda \frac{\partial T}{\partial r} = (T^* - T)\alpha \qquad \text{at} r = R \tag{VI.105}$$

where α is heat transfer coefficient at the filament surface. If we replace r with p in equation VI.105 then

$$\frac{\partial T}{\partial p} = (T^* - T)\frac{R\alpha}{\lambda} = (T^* - T)Nu \tag{VI.106}$$

where Nu is Nusselt number. Also, at the time zero the temperature of all the elements is equal the temperature of extrusion. The average value of the heat transfer coefficient for perpendicular flow of cooling air denoted here as $\bar{\alpha}$, Kase and Matsuo[30] defined as

$$\bar{\alpha} = 0.473 \cdot 10^{-4} A^{-0.667} Q_m^{0.334} \rho^{-0.334} \left[1 + \left(\frac{8\rho A}{Q_m} v_y\right)^2\right]^{0.167} \qquad \text{(VI.107)}$$

where A is cross sectional area of the filaments, v_y is velocity of air perpendicular to the filament. The value of $\bar{\alpha}(x)$ may be calculated using equation VI.107.

As the Nusselt number varies around the periphery of a cylinder, Matsuo and Kase adjusted their average Nusselt number calculated according to equation VI.107, and calculated the angular dependence using the determinations, reproduced here in figure VI.18, of Eckert and Soehungen[29] for a stationary cylinder. A so calculated Nusselt number was expressed as a ratio $\alpha/\bar{\alpha}$. Naturally, it is a major simplification, but a more correct determination of the Nusselt number is not known even today, leave alone then, in the year 1975 or so.

To solve the equation, Matsuo and Kase considered one half of the filament cross section and divided it as shown in figure VI.19. In devising the solutions, the following assumptions were made:

- Each of the 81 segments considered is assumed to have a uniform temperature.
- The overall heat transfer coefficient at the filament surface is equal to

$$\left(\frac{R\bar{\alpha}}{\lambda}\right)\left(\frac{\alpha}{\bar{\alpha}}\right) = \frac{R\alpha}{\lambda}$$

  with the values used as functions of X and β.
- The air flow direction coinciding with the diameter line 0° - 180° is the symmetry line, and as such is non-conducting.
- The heat transfer between two adjacent elements was determined to be $\lambda/distance$ between centers of the two adjacent elements.

The difference equation resulting from the above derivations was given the following form[28]

$$\frac{T^*_{i,j} - T_{i,j}}{\Delta X} = \frac{T_{i+1,j} - T_{i-1,j}}{2p_i \Delta p} + \frac{T_{i+1,j} - 2T_{i,j} + T_{i-1,j}}{\Delta p^2} + \frac{T_{i,j+j} - 2T_{i,j} + T_{i,j-j}}{p^2 \Delta \beta^2} \qquad \text{(VI.108)}$$

If we replace the arc length $p\Delta\beta$ by Δq, equation VI.108 receives a form

$$(\Delta p \Delta q)\frac{T^*_{i,j} - T_{i,j}}{\Delta X} = \Delta q \left(1 + \frac{\Delta p}{2p_i}\right)\frac{T_{i+1,j} - T_{i-1,j}}{\Delta p} +$$

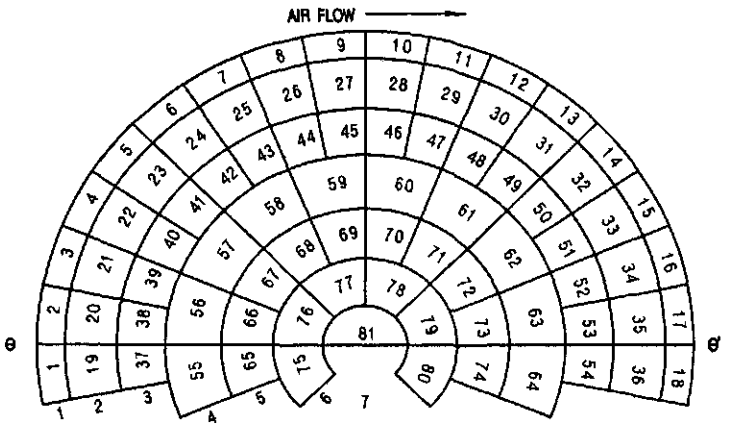

Figure VI.19: *Division of a filament cross section into elements. After R. Matsuo and S. Kase.*[27,28]

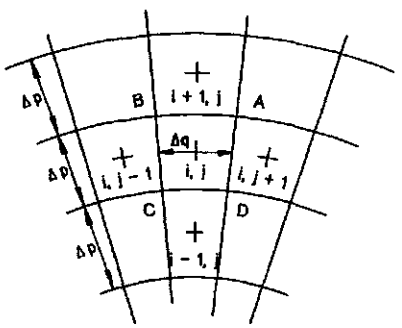

Figure VI.20: *Scheme of differencing in the cylindrical coordinates. After S. Kase.*[28]

$$+\Delta q\left(1-\frac{\Delta p}{2p_i}\right)\frac{T_{i-1,j}-T_{i,j}}{\Delta p}+\Delta p\frac{T_{i,j+1}-T_{i,j}}{\Delta q}+\Delta p\frac{T_{i,j-1}-T_{i,j}}{\Delta q} \qquad \text{(VI.109)}$$

Figure VI.20 serves as a visual aid to equations VI.108 and VI.109. The designations here are: $T^*_{i,j}$ is temperature of the cooling air, ΔX is the difference increment in X, the dimensionless distance from spinnerette. Here $\Delta p \Delta q$ gives the volume of the center element i, j assuming the thickness of the "disk" is unity, $\Delta q(1 + \Delta p/2p_i)$ is the arc length AB, Δp is the wall length $DA = BC$, and $\Delta q(1 - \Delta p/2p_i)$ is the arc length CD. The heat transfer coefficient at walls AB and CD is equal to the inverse of Δp and for walls DA and BC it is the inverse of Δq.

Examples of the computational results by T. Matsu and S. Kase are given in figure VI.21. These results were corroborated semiquantitatively by a dying test; the shape of the dyed segments coincided with the calculated results. However, there is no positive test available yet to determine such nuances with a full quantitative certainty.

The method of calculations may serve well for theoretical considerations of many problems. Naturally, better ways of determination of the heat transfer

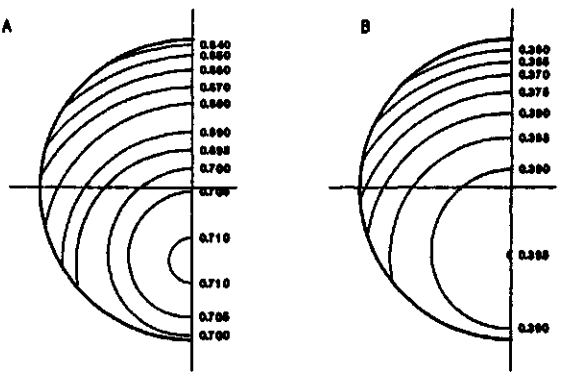

Figure VI.21: *Cross flow quench: mapping of isotherms in non-dimensional temperature in a fiber cross section, A. 2 cm from spinnerette, B. 12 cm from spinnerette. Melt temperature 260°C. After T. Matsuo and S. Kase.*[27,28]

coefficient are badly needed to allow more faith to be put into results calculated by any method.

VI.2.b Equipment

Quenching

Some comments on quench equipment have been made in the subsection on quench systems and all along the chapter on Engineering Physics. By now we are able to conclude that there is a fair amount of important design data which may be calculated. The point is: where are the pitfalls?

The difficult problems lacking adequate solution are connected to multi-filament operations, particularly the aerodynamic problems and the related estimation of heat transfer coefficients. Specifically, attention is to be paid to the pumping action, that is, to the boundary layers around a multi-filament spinline of variable filament-to-filament distance. Since with multifilament operations the most often used quench system is a cross flow of air, the mutual influence of the pumping action (i.e. the flow parallel to the spinline, and the cross flow) is of paramount importance. Thus far, these areas require heavy and expensive experimental support and careful observation of the aerodynamic and heat exchange phenomena from the initial experiments all the way through the scaling up. Szaniawski and Zachara[56] developed a quantitative solution for the entrenchment problem in wet formation. The principles of the solution are treated in section VII.3. It appears that the solution may be adapted to air systems.

In work with rapidly crystallizing polymers, or when aiming at very high modulus fibers, it may be advisable to use liquid (water) quench. Understandably, this is connected to small housekeeping problems, but sometimes it is worth the effort.

As it results from the polymer habits in fiber attenuation, location of the liquid surface very closely to the spinnerette face is rather an ill advised idea. If

the crystallization process is to be retarded, then the maximum of the attenuation work ought to be spent at a temperature where relaxation time is shorter and the temperature is also too high for the crystallization to begin, even with a work input. At the moment of the first contact between a filament and the water surface, the amount of stored work should be as small as possible. To achieve such conditions, a *delayed quench* may be recommended as a good solution. After the attenuation is done under proper conditions, rapid water quench may achieve the desired goal.

In the case of water, due to higher density and higher viscosity, the problems related to the fluid dynamics are substantially aggravated. The frictional drag on filaments is much greater, and this requires special care in the management of synchronization of the stress and temperature profiles along the spinline. Due to the very large pumping action, high filament speeds are rather impossible. If a process needs to be intensified, it is to be achieved through an increase of the number of filaments. The theoretical solution of Szaniawski and Zachara[56] may be very helpful in the design work of liquid quench.

It should also be observed that certain liquids may influence the crystallization process in some polymers. Usually such influences have negative results, sometimes so much as to prohibit the application of a particular liquid.

Neck Drawing and Annealing.

For good control of fiber properties and for good reproducibility of any process of fiber formation, it is quite essential to have as good control of the neck drawing temperature as possible. This is automatically connected with the control of the neck localization.

In the past, the neck was localized with the use of a *pin* over which the fibers were drawn. Initially, when a relatively relatively small number of filament were produced in one position, the filaments coming either from bobbins or directly from formation, were wound around *the pin*, a thin metal bar, and drawn by a set of rollers rotating faster than the fibers were fed. In this way the neck was localized within only a few millimeters of the filament travel. Nonetheless, this solution had serious drawbacks. The large friction, with its additional force requirement, caused excessive filament breaks. Equally detrimental was the heat generated by friction, in addition to the heat generated by the drawing itself.

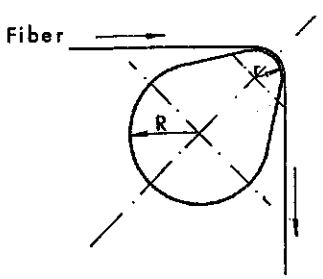

Figure VI.22: *Pin for neck drawing of multifilament threadlines.*

With time, the pins have changed to larger bars, as in figure VI.22, often with a cross section reminiscent of a pear, with cooling channels inside to remove the excess heat generated by the operation. In terms of fiber properties, such a system worked well, but the breaks, a serious problem of the process economy, still showed to be too high. With the passing of time, localization of the neck zone came to be realized only through temperature control.

The most frequently used heaters are contact heaters with a somewhat curved contact surface, as it is shown schematically in figure VI.23. The fiber guides located under the heater are often regulated by the threadline tension. In this way, an increase in tension moves a guide so to increase the length of contact between the fibers and the hot surface. The contact surfaces are plated either with chrome or with aluminum oxide; various degrees of smoothness (or grain) of the surfaces are used to adjust the heat transfer and the friction.

The convective heat transfer from the air is usually higher than the direct heat transfer between the fiber and metal surface, aside from the small area of contact between the flat metal surface and a fiber cylinder of tiny diameter. Because of this, the contact surfaces are often ribbed or grooved to enhance the heat exchange.

Such surface heaters usually have a vapor-condensation system for heating with maximum uniformity of temperature distribution. Nevertheless, such heaters heat the fibers from one side only and introduce an element of asymmetry, which sometimes may be undesirable.

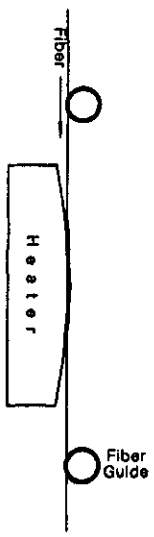

Figure VI.23: *Contact plate heater for neck drawing of fibers, schematic representation of a cross section.*

The asymmetry in heating, as well as undesirable friction, may be avoided by using heaters which utilize air. A schematic drawing of two such gadgets are reproduced in figures VI.24 and VI.25. Utilization of such solutions is particularly well suited when drawing is conducted in more than one stage, as the second (and

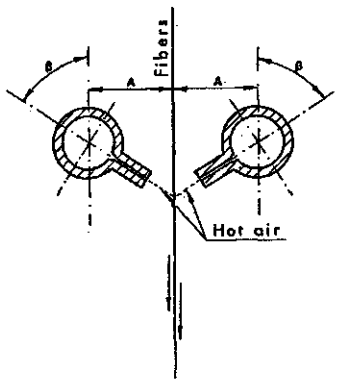

Figure VI.24: *Schematic representation of a gadget for localization of fiber drawing in jets of hot air.*

possibly third) stage drawing is usually conducted in *tunnel heaters* which are non-contacting – air is the heat transferring medium.

There are drawing operations utilizing heated rollers, the same rollers which are used to transport the threadline. Occasionally they work adequately, though it is not a solution worthy of recommendation. The drawing operation often starts before the fibers leave the roller. In effect there is a slip-stick vibration on the last ninety or so degrees of the wrap angle. This cannot be considered as an enhancement of the fiber quality.

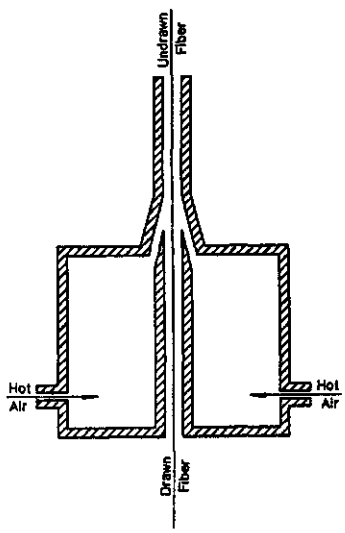

Figure VI.25: *Schematic representation of drawing in a stream of hot air.*[31]

If a neck drawing operation is conducted in more than one stage, the operations must be separated by rollers which appropriately control the tension in the zones. The journey from drawing heater through the rollers causes a change of fiber

temperature, and this must be taken in the consideration.

Immediately after neck drawing, fibers may be subjected to a heat treatment with the purpose of annealing of the fiber structure, or controlled post draw relaxation to avoid the crushing of the bobbins on which the fibers are ultimately wound up. Such an heater, depending whether the operation is to be isometric or not, may be preceded with rollers in analogy to multistage drawing steps. All the heaters, whatever their purpose, located after the first stage and localization of the neck consist of some kind of tunnel heater, as mentioned above.

As the contemporary fiber formation operations are very fast, residence time in such in-line heaters is usually very short. To go around this problem a *shock heating*[32] is often used: an exposure of fibers to a temperature higher than the fiber melting point. Such a high temperature helps the heat transfer, the fibers never reach their melting point in the available time. However, provisions for effects of possible fiber breaks ought to be here in place.

VI.3 Mass Transport

VI.3.a Polymer Transport

Practically all the fiber formation equipment now uses extruders for melting and transporting the polymer being fed into the system. Also, in cases where the formation operation is supplied directly from continuous polymerization units, extruders of one type or another are used for transporting the melt. The theory of extrusion and the design of the equipment have been described extensively elsewhere.[33–36] Similarly, design of metering pumps will not be described here, as it is a specialty of several manufacturers and the reader is referred to their literature.

The feeding of polymer to the formation machines, aside from melting it in the extruders, requires heated piping to deliver the polymer to the *spinning block* or *spinning beam*. (The nomenclature in the field varies substantially.) The difficult question of maintaining uniform temperature across the larger diameter pipes was treated by Saltuk et al.[37] The authors treated a power law non-Newtonian fluid moving through a circular duct. It was found that the viscous heat dissipation is a function of the Graetz number, and for values larger than seven the heat generated by flow may constitute a problem.

Filtration of polymer melt represents an important part of the formation process. Despite this importance, the subject has found little treatment in literature. The only significant review was published by J. G. Savins[38] for polymer solutions.

In the engineering of a fiber formation process, one of the essential questions is the drop of pressure on the filtering medium. For filtration, different media may be used: sand, sintered metal, steel balls, or metal screens. The final construction of a filtering system is usually a result of a compromise between the need for polymer homogenization, the quantity and type of impurities which like to clog the filters, and the pressure requirement to force the polymer through the filter. The

pressure requirement is important for the cost of equipment, the clogging has a bearing on the process economy through increase of the down-time. Quite often, however, the gains of reduced filtering efficiency are illusory since the poorer filtration usually leads to increased filament breaks. The two technologically important arguments which may limit the tightness (or shear) of the filter are: not to exceed the threshold of the degrading shear; and not to reach too high a pressure, which may be connected with problems of building high pressure equipment and with the high costs connected with it. The degrading shear rate is a polymer property depending on molecular mass (see chapter on rheology).

Some filtering materials may be tested experimentally in slightly modified capillary rheometers. Otherwise, calculations are a possibility. Generally, the most convenient way is to start from the general equations of Poisseuille (capillary) flow:

$$F(\tau_w) = \frac{v}{r} = \frac{1}{\tau_w^3} \int_0^{\tau_w} \tau^2 \dot{\gamma}(\tau) d\tau \tag{VI.110}$$

$$\eta = \frac{\tau_w}{4F(\tau_w)} \tag{VI.111}$$

where $F(\tau_w)$ represents the function of shear stress at the tube (capillary) wall, v is average velocity, r is tube radius, shear stress at the tube wall $\tau_w = r\Delta P/2L$, ΔP is pressure difference needed to force the fluid through the tube, L is tube length, $\dot{\gamma}$ stands for shear rate, and η means fluid viscosity. For filtering materials, the tube radius may be substituted with the *hydraulic radius* r_h, which in this case is defined as

$$r_h = \frac{d_p \epsilon}{6(1-\epsilon)} \tag{VI.112}$$

where d_p stands for particle diameter (e.g. in case of sand), and ϵ is porosity or void fraction. Some further relations are

$$r_h = \frac{\epsilon}{S} \tag{VI.113}$$

$$\frac{S}{S_0} = 1 - \epsilon \tag{VI.114}$$

$$d_p = \frac{6}{S_0} \tag{VI.115}$$

Here S is wetted surface per unit volume of the porous material, and S_0 is total surface of particles in unit volume of the porous material.

Usually the channels present in a porous material are not straight, and it is necessary to correct for this fact by introducing a coefficient c' to multiply the tube length L.[39] After applying the correction, one may rewrite equation VI.110 in the following form.

$$F(\tau_w) = \frac{3(1-\epsilon)v_0}{d_p \epsilon^2} = \frac{1}{\tau_w^3} \int_0^{\tau_w} \tau^2 \dot{\gamma}(\tau) d\tau \tag{VI.116}$$

where *superficial viscosity*, $v_0 = \epsilon\langle v\rangle$, and $\langle v\rangle$ is pore velocity.

$$\tau_\epsilon = \frac{\omega \Delta P}{6c'L} \tag{VI.117}$$

$$\omega = \frac{d_p \epsilon}{1-\epsilon} \tag{VI.118}$$

The *Darcy viscosity*[38] is

$$\eta_\epsilon = \frac{\tau_\epsilon}{4F(\tau_\epsilon} = \frac{\omega^2 \epsilon}{72c'} \frac{\Delta P}{v_0 L} \tag{VI.119}$$

When comparing the flow curves obtained for capillary flow with those for the porous layers, the latter ones are shifted by a factor of c'. It is assumed that neither the flow conditions nor the flow character changes.[38]

Essentially the same solutions, though in somewhat different form, have been published by other authors.[39,44]

In general, the agreement between experiment and calculations conducted according to the above given method are within $\pm 10\%$,[38,43] however larger deviations are observable. Such larger deviations are interpreted as resulting from a strongly elastic character of the polymer, or adsorption of the polymer on the surface of the filter material, or on simple clogging of the channels by impurities of different nature.[44,47] In some cases, it is referred to as a formation of gel on the porous surfaces,[47] though collection of gel has been proved experimentally,[48] and so it appears more likely a collection rather than a formation.

The pressure drop accompanying the passage of a viscoelastic liquid through a porous layer may be obtained by performing the calculations as for a Newtonian fluid, then the result is to be corrected as follows.[44,49]

$$\Delta P_{viscoel} = \Delta P_{viscous} \left[1 + A\left(\frac{\theta v + 0}{\epsilon d_p}\right)^2\right] \tag{VI.120}$$

where A is a constant between 5 and 10, θ is relaxation time.[50]

Since there is some uncertainty of whether a given polymer obeys the rule allowing the recalculation or not, it may be highly recommended to make an experimental check whether equation VI.116 holds. If the filtration medium has a propensity for adsorption of polymer in use, then the filtering material is unsuitable for the process. Complete chemical and physicochemical inertness of a filtering material is the primary criterion for its application.

Immediately below the bottom surface of the filter, a certain free space should be left as a flow equalizer before the polymer enters the spinnerette.

VI.3.b Spinnerette Design

A successful design of a spinnerette requires a good knowledge of the melt flow characteristics of the polymer to be used. The most informative in this case

appear to be the oscillatory experiments, though capillary experiments should also be considered for the sake of determination of die swell. Die swell is always somewhat enigmatic and changeable, calculations do not seem to suffice for good design. It is true that the small entrance angles are preferred, but an experimental check on the effects of the entrance cone angle may be worth the little extra effort.

From the rheological measurements in capillaries one may select the smallest aspect ratio which will still permit operation on the flatter portion of the curve representing the swell-aspect ratio relationship. Flow in short capillaries is normally connected with steeper dependence of the die swell on the aspect ratio, therefore slight inaccuracies in the length of different capillaries in a spinnerette may cause excessive variations between the diameters of different filaments.

The level of shear rate during extrusion through a capillary also affects the fiber quality. Generally, a higher level of shear rate leads to tougher fibers with more stable structure, therefore it is technologically advisable to use the highest shear, though staying within some reasonable limits. The limitations on the shear rate are here the same as in the case of filters.

Further, the flow considerations must be based on the simple balance of the material flow throughout the entire process of formation.

$$Q\rho_0 = \frac{\pi d_0^2 v_0 \rho_0}{4} = \frac{pid_1^2 v_1 \rho_1}{4} = \frac{\pi D_S^2 v_S \rho_s}{4} = \frac{\pi d_f^2 v_f \rho_f}{4} \tag{VI.121}$$

where Q is volumetric polymer flow rate, ρ represents polymer density, v is velocity of the polymer stream, and d is diameter of the polymer stream. The subscripts denote: 0 – in capillary, 1 – in the die swell at maximum diameter B, s – in undrawn fibers, and f – in drawn fibers. And as a reminder, *spin stretch*, $SS = v_s/v_1$, draw ratio, $DR = v_f/v_s$. Draw ratio must be corrected for the amount of post draw relaxation to assure arriving at the desired final fiber thickness. One may also use the material balance so as to arrive at the weight titer of the fibers, denier or decitex:[‡]

$$Q\rho_0 = Q_w = \frac{(dpf)_f}{9000} = \frac{(dTx)_f}{10000} \tag{VI.122}$$

After simple arithmetic, one may arrive at a useful formulation like

$$Q\rho_0 = 1.389 \cdot 10^{-3} \frac{d_0\dot{\gamma}}{B}(dpf)_f)(SS)(DR) \tag{VI.123}$$

The rest of the flow calculations are identical to those described for the flow in capillaries in the chapter on rheology. The strength of the spinnerette plate itself, as well as the mounting, are matters for mechanical engineers.

A point of much discussion is the distribution of holes in multifilament spinnerettes. The only theoretical guidelines are those that result from the aerodynamics. Naturally, the larger the distance between the capillaries the better, however,

[‡]Denier = dpf = weight in gram per 9000 m fiber; Decitex = dTx = weight in gram per 10000 m fiber.

this leads to a large size of spinnerette plate, and this requires thicker spinnerettes for the sake of strength and resistance to buckling.

In co-current axial air flow, the filament-to-filament differences are relatively small, though nothing concrete is known about a flow around converging filaments. At least the general direction of flow is the same for fibers as it is for the cooling air. Much more complicated are the matters for cross flow quench. The first row of fibers in the air path has higher flow velocity and cooler air. For each of the following rows of fibers the cross flow velocity is smaller due to the pressure drag and the pumping action, and at the same time each following row experiences higher temperature of the cooling air. In result, the fiber-to-fiber differences are large. The best distribution of holes is such which diminishes the adverse effects to the bare minimum, whatever this means.

For really large spinnerettes, a helpful way to decrease the nonuniformities may be to change from the traditional round spinnerettes to rectangular plates. In this way, there may be fewer rows of filaments, and this means fewer obstacles for the air to overcome. Additionally, the rectangular spinnerette may be helpful in reducing the plate thickness and increase the circumference to area ratio which is of importance in the strength of the spinnerette mounting.

VI.3.c Filament Transport

The term filament transport here means not only transport. In a common downward formation system, gravity would be sufficient to move the fibers. The transport must also have some muscle, it must provide force for diameter attenuation and force for neck drawing in integrated processes. The most frequent way of satisfying the strong transport needs is by way of rollers or *godets*. (Again, the nomenclature varies from place to place.) The other means — air jets are used almost exclusively for *spunbond processes*. Jets have been discussed in the section on aerodynamics.

Before the fibers solidify they are guided contactless through the air. The first contact is possible only after solidification, or glassification. The oldest and the most popular way is to wrap the threadline several times around a pair of rollers driven in the same direction. To prevent the threadline from jamming together or falling off the axes of the two rollers in one pair must be canted some five to twenty degrees. Often, particularly for smaller threadlines, like those for continuous filaments, the second roller is not driven – it is just a free wheeling *separator* roller. The nonparallel alignment of the roller axes causes the threadline to follow a spiral-like path. Such system, is often referred to as a *multiple wrap system* and is a convenient way of threadline transport. The multiple wrap is advantageous for threadlines under high tension because the higher the tension, the stronger the threadline clamps around the pair of rollers. Multiple wraps may give 1440°, or more, wrap angle. Theoretically, for constant filament diameter and fiber- roller coefficient of friction, the frictional force depends only on the wrap angle.

If there is a large number of filaments produced on one position, then application of the multiple wrap is difficult. Starting from about two hundred filaments and up, though the limit may depend also on the local filament diameter, the multiple wrap system requires excessively long rollers. Very long rollers pose problems for the designers, and, more importantly, they may also represent a safety hazard for the operators. Additionally, the really large threadlines on multiple wrap have an increased tendency to form uncontrolled fiber entanglements. A parallel alignment of the filaments during the transport is very important, overlapping fibers lead to an reduction of frictional force. If the spinline is meant to be intertwined, then it is made under controlled conditions, in the proper place in the process; it concerns usually smaller threadlines, anyhow. The matter of fiber uniformity is of constant concern, however, uncontrolled entanglements at improper points of the process may represent a threat to the fiber uniformity and to the filament break levels. The multiple wrap system always bears the danger of disobeying all the above interdictions, and with larger tows, the dangerous possibilities quickly become certainties.

The majority of vices inherent in the transport with multiple wraps around two rollers may be avoided when using the so called S-wrap system. Figure VI.26 presents the principle of the S-wrap geometry. Rollers are arranged in pairs, as in the multiple wrap system, however, their axes are exactly parallel and the rollers rotate in opposite directions. Both of the rollers must be driven. The threadline is guided through the roller surface in an S-like pattern. Although this way of guiding fiber tow is free of the vices characteristic for the multiple wrap irrespective of the size of the tow, it is connected with a problem of its own. There is a limit to the wrap angle. One pair of rollers may give a maximum wrap angle of only some 440°.

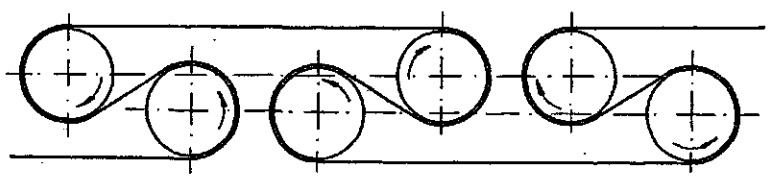

Figure VI.26: *Schematic representation of the S-wrap system for fiber transport.*

Figure VI.27 shows the details of the geometry of an S-wrap. The wrap angle around one roller, δ, may be formulates as

$$\delta = 270° - (\lambda + \alpha) \tag{VI.124}$$

where

$$\alpha = \beta - \delta \tag{VI.125}$$

and β is the roller alignment angle. The other relationships of importance are

$$\sin\lambda = \frac{b}{2a} = \frac{b}{(2r + c)} \tag{VI.126}$$

and

$$\cos\alpha = \frac{r}{a} = \frac{2r}{(2r+c)} \tag{VI.127}$$

where b represents distance between the roller surface and the bypassing threadline, $a = r + 0.5c$, c stands for distance between the roller surfaces.

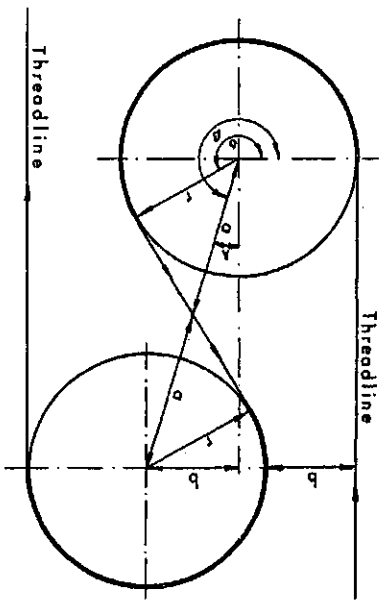

Figure VI.27: *Geometry of the S-wrap rollers. Different relative positions of the roller axes permit variations of the wrap angle δ.*

For the fibers to be laced up, it is necessary for b and c to be at some minimum size, usually the distances cannot be smaller than about 5 *cm*, though for heavier tows or for longer rollers it may be necessary to have the b and c larger than 5 *cm*. Usually, the dimensions of b and c are kept equal, and in such case the condition to obtain the maximum wrap angle of $\approx 440°$ is $b = c = 0.55\ r$.

When a reasonable increase of the roller diameter does not suffice and the wrap angle still must be increased, then wrapping may be realized only by using multiple pairs of rollers, and this may become an expensive proposition. It is self-evident that maximum utilization of any given wrap angles requires that the roller surfaces be made of a material with as great as possible coefficient of friction with the fibers in question.

The coefficient of friction varies substantially for different pairs of materials, and it is often not easily predictable. It varies even for certain variables other than just the surface quality. G. W. Schael[51] described the static coefficient of friction between surfaces of polypropylene film. These results are reproduced in figure VI.28: coefficient of friction f_s is given as a function of the degree of crystallinity expressed as density. Naturally, the friction coefficient depends also on the degree of gloss of the surface, *e.g.* line A in figure VI.28 represents film with a higher

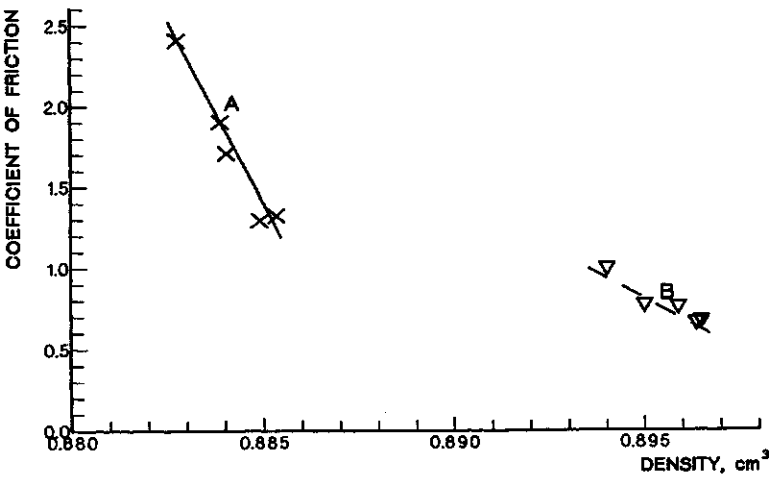

Figure VI.28: *Influence of crystallinity, expressed as density, on the coefficient of friction between the polypropylene film surfaces. A: a film of higher gloss than in case B. After G. W. Schael.*[51]

gloss than that represented by line B. The quantitative data published on the subject are rather scarce. Nonetheless, the differences of the coefficient of friction in relation to the degree of crystallinity or fiber elasticity, or fiber softness, are well realized in industry and in theory.[52,53]

A relatively extensive study of friction of polyamide yarn has been conducted by G. A. Gol'ubyev and co-workers.[54] Their results are quoted here in figures VI.29 and VI.30. Figure VI.29 presents the relationship the authors have found between the friction coefficient, diameter of a roller, and threadline tension. The influence of roller diameter on the coefficient of friction is rather difficult to explain theoretically; on a rough surface the influence of diameter is significant only at low tension (plane A in figure VI.29), while on a glossy surface, a lesser degree of influence was noticed over the entire investigated range of tensions (plane B in figure VI.29). The technological importance of the influence of tension on the coefficient of friction does not require particular stressing.

The influence of velocity on the coefficient of friction of polyamide fibers on a matted surface is shown in figure VI.30. The influence of velocity goes through a maximum at 350 to $400 m/min$ and overpowers the influence of fiber tension. The importance of these results does not require any additional emphasis.

The parameters investigated by Gol'ubyev and co-workers do not represent all the parameters which influence friction. The material of the roller surface represents a very strong factor. The most often used surfaces are chrome and aluminum oxide, both with a wide range of gloss, or grain. In special cases, roller surfaces made of various ceramic materials or rubber may be the most appropriate.

Since the degree of crystallinity and the majority of fiber properties change along the fiber path, in some cases it may be necessary to use different kinds of surfaces at different points of a machine.

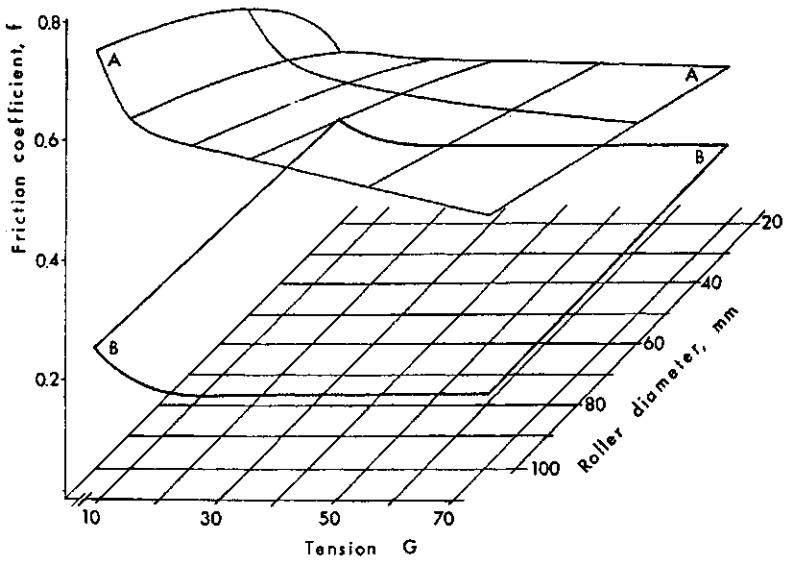

Figure VI.29: *Influence of fiber tension and roller diameter on the coefficient of friction with polyamide fibers. Plane A – glossy roller surface, plane B – rough roller surface. After G. A. Gol'ubyev and co-workers.*[54]

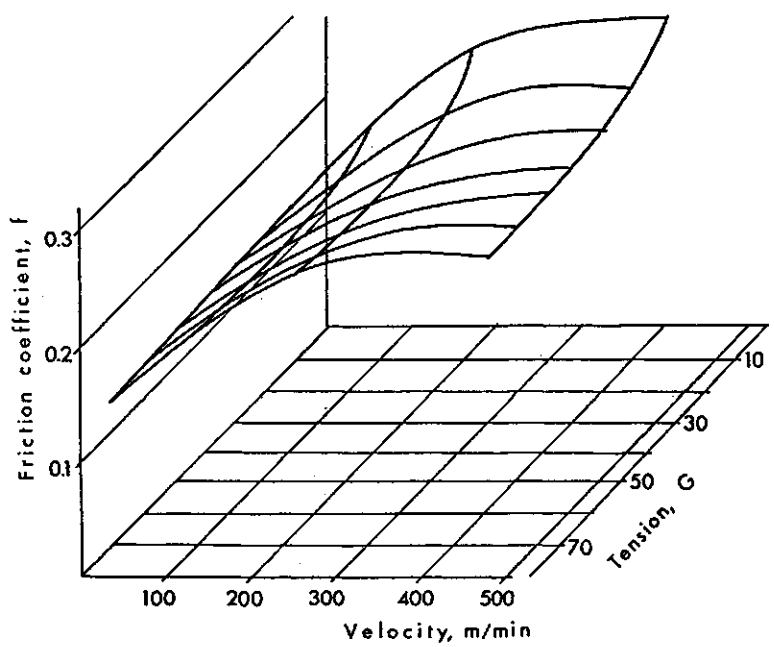

Figure VI.30: *Influence of polyamide fiber velocity and tension on the coefficient of friction with a matted chrome surface. After G. A. Gol'ubyev and co-workers.*[54]

It is quite obvious that the rollers of the drawing zone represent much more critical demands since they have to overcome much higher threadline tensions.

The hardware for transport of fibers does not consist only of driven rollers: various types of threadline guides form another separate group.

- Guides which serve to change the direction of threadline.
- Guides which spread fibers in a monofilament layer.
- Non-rotating guides.

The rotating guides may be divided according to their geometry:

The guides of the first group represent usually undriven *cylindrical* rollers of rather small diameter on the order of 25 to 100mm. If they do not have their own mechanical drive, then they are driven by the moving threadline, and in such cases should pose a minimal resistance, thus low mass and good ball or roller bearings.

The second group consists almost exclusively of undriven rollers of still smaller diameter, ranging from some 20 to $max.$ 75mm. Their characteristic attribute is the not quite cylindrical, but rather *barrel-like surface.* This barrel-like surface spreads a tow in a layer of single filaments, almost like a ribbon, without overlapping. Exaggerated bellowing of the guide surface may lead to excessive spreading, all the way to leading the filaments off the transporting rollers. The guides usually work in the immediate vicinity of the driven rollers.

The non-rotating guides, usually in the form of "pig-tails", rings and eyelets, are made either of steel, or ceramic surfaces on metal support. They are useful on small threadlines. On large tows they are to be avoided. Use of them in the contact with undrawn fibers is "prohibited".

The last segment of the transport arsenal are winding machines which are manufactured by companies specializing in such equipment. The winders work either with constant fiber velocity or with constant fiber tension. The manufacturers' literature is to be consulted for details of this equipment.

VI.3.d Machine Geometry

The term *machine geometry* used here represents the notions which pertain to the description of the relative positions of the technologically important elements of a fiber forming machine, spinnerette, take-up rollers (or jets), draw rollers, relaxing rollers, winding, guides, *etc.* This notion is essential to the process of formation, not only because of a space requirement.

One of the most important aspects of machine geometry is the fact that the distances together with fiber velocity profile determine time, and residence time. Fiber formation is a process, and as a process it runs in time. The availability of time determines then *how* and *how far* the physical processes involved in fiber formation may go. A change of the time scale automatically changes the whole process. For this reason, for a given process the time scale, also the machine

geometry, cannot be changed, or scaled up or down. If the geometry is changed, the process is changed, and the product properties will change.

In the machine geometry there is a delineation of different zones. The following criteria may be adapted as the definitions of the different zones.

• **Quench zone** encompasses the distance from that point below the spinnerette where the extruded filament reaches maximum diameter (die swell), which is usually one half of the fiber diameter. The end of a quench zone is at the point where the process of polymer crystallization is completed. It is a gross misconception that the quench zone stretches all the way to take-up rollers (or jets). The distance between the end of crystallization and the take-up rollers is simply a "no man's land", it represents certain length of time where the fiber is left under tension and out of control. The take-up rollers represent a border, a transition point, a necessary evil; if they are heated and prepare the fibers for drawing – then it is a draw zone. When quenching and drawing are performed in separate operations, paradoxical as it may sound, the storage of undrawn fibers belongs to the process, to the "no man's land" and out of control.

• **Drawing zone** stretches from the point where the fiber is subjected to a drawing tension, and this usually coincides with heating to a drawing temperature. The zone ends at a point where the tension exerted on the fiber is smaller than the drawing tension, be it for relaxation, for winding or for cutting. Sometimes a drawing zone may be divided into several stages; in such case only the first stage may have localized neck. Some of the ultradrawing processes may require multiple zones with gradually increasing temperature.

• **Annealing** or **stabilization zone** is the space where the fiber becomes subjected to an elevated temperature while under constant length, or when the extension is very small. This last possibility becomes similar to an additional stage of drawing, the main difference being that in drawing, fibers are exposed to heat over limited areas, while annealing uses the longest possible residence time. During drawing, some heat is generated within the fiber; in annealing no heat is generated in the process and the fiber temperatures may be significantly higher than drawing temperatures for a given fiber.

• **Relaxation zone** stretches from the end of the drawing zone, sometimes it encompasses also annealing, and it ends just before the winding of the fibers, or before any other point of removing the fibers from the process. Neck drawing is rather a brutal operation, after which the fibers, even after annealing or stabilization, have a tendency to relax and shrink. The exception may represent processes with very modest draw ratios. Normally, relaxing fibers shrink some five per cent. In extreme cases, the shrinkage might be as high as ten per cent. The purpose of the relaxation zone is to alow the fibers to shrink either to a predetermined degree or to a desired tension. Occasionally, relaxation may be divided into several zones. Fibers produced for cutting into staple are rarely subject to a relaxation under controlled conditions.

The "no man's land" may not be limited just to quench zones. It may be found in all other places as well. A "no man's land" in the quench zone is usually the

most harmful, besides being equally, or even more, costly as in all other points.

Another question, though sometimes controversial, is whether the threadline should be transported vertically or horizontally. From the point of view of economy, the vertical configurations are much more desirable. Land in industrial parks is getting more and more expensive. Technologically, the verdict ought to be the same since the threadline moves in the natural direction following the force of gravity. In horizontal configurations, the threadline is subject to the gravitational forces acting at a normal to the direction of fiber motion; this causes snag or bellowing of the filaments, which usually aids vibrations and threadline fluttering. The harm of a horizontal configuration grows with the growing distances between rollers or other points of support. Operational convenience may sometimes require horizontal configurations, but there are not many processes which would require such particular kinds of machine geometry, naturally, aside from the wet formation from solution.

A mixed configuration, with the drawing segment below take-up rollers arranged horizontally are more frequent. The horizontal position does not pose as many harms to fibers under higher tension.

Machine vibrations, were mentioned earlier at several points. Their main sources are the rotating elements of the machine, particularly those rotating at high rates of speed, and those involving powerful motors. Inaccuracies in balancing rollers or motors cause the vibrations, which may be easily transmitted to the threadline. Though somewhat less dangerous, but still worth taking into account, are building vibrations. The latter are usually of low frequency and are caused by heavy equipment like extruders, climatization, air compressors, *etc.*

VI.4 References

1. J. Łukasiewicz, Jr., *private consultations.*
2. S. F. Hoerner: *Fluid - Dynamic Drag*, published by the author, Washington, D. C., 1958, Chapter 3.
3. B. C. Sakiadis, *A. I. Ch. E. Journal*, **7 (1961)**, 26, 221, 467.
4. Y. Sano and K. Orii, *Sen-i-Gakkaishi*, **24 (1968)**, 212.
5. L. R. Glicksman, *Trans. A. S. M. E.*, **paper No 68-FE-19.**
6. M. Matsui, *Trans. Soc. Rheol.*, **20 (1976)**, 465. 56.
7. Y. D. Kwon and D. C. Prevorsek, *Trans. A. S. M. E.*, **paper No 76-TEX-7.**
8. J. Gould and F. H. Smith, *J. Text. Inst.*, **(1980), No. 1**, 38.
9. S. Middleman and G. Vasuvedan, *A. I. Ch. E. Journal*, **16 (1970)**, 614.
10. F. M. White: *Viscous Fluid Flow*, McGraw-Hill Publ., New York, 1974.
11. E. M. Sparrow, H. Quack, and C. J. Boerner, *A. I. A. A. Journal*, **8 (1970)**, 1936.
12. R. E. Sayles, *A. I. Ch. E. Journal*, **36 (1990)**, 1917. 12.
13. E. H. Andrews and D. L. M. Cansfield, in *Fibre Structure*, ed. by J. W. S. Haerle and R. H. Peters, Butterworth Publ., London, 1963, p. 487.
14. A. Selwood, *J. Text. Inst.*, **53 (1962)**, T573.

15. Z. K. Walczak, *previously unpublished*
16. A. Dutta, *Polymer Eng. Sci.*, **27 (1987)**, 1050.
17. A. Dutta, *Text. Res. J.*, **57 (1987)**, 13.
18. J. Lukasiewicz, Jr., *Aircraft Eng.*, **(1947)**, 55, 86.
19. L. Prandtl: *Essentials of Fluid Dynamics*, Blackie & Son Publ., London, 1952.
20. E. H. Andrews, *Brit. J. Appl. Phys.*, **10 (1959)**, 39.
21. J. Hennig, W. Knappe, and F. Lohe, *Kolloid Z.*, **189 (1963)**, 114.
22. T. R. Fuller and A. L. Fricke, *J. Appl. Polymer Sci.*, **15 (1971)**, 1729.
23. G. Wilhelm, *Kolloid Z., Z. Polymere*, **208 (1966)**, 97.
24. E. L. Albasiny, *Quart. J. Mech., Appl. Math.*, **13 (1960)**, 374.
25. J. Crank and P. Nicolson, *Proc. Camb. Phil. Soc.*, **43 (1947)**, 50.
26. J. Shimizu, K. Shimazaki, K. Toriumi, and T. Mitsui, *J. Text. Mach. Japan*, **18 (1972)**, 125.
27. T. Matsuo and S. Kase, *J. Appl, Polymer Sci.*, **20 (1976)**, 367.
28. S. Kase, *J. Appl. Polymer Sci.*, **27 (1982)**, 2729. 28.
29. E. R. G. Eckert and E. Soehungen, *Trans. Amer. Soc. Mech. Eng.*, **74 (1952)**, 343.
30. S. Kase and T. Matsuo, *J. Appl. Polymer Sci.*, **11 (1967)**, 251.
31. *Jap. Pat.* No. 21,566 (1966), to Sekisui Chem. Ind.
32. P. H. Geil: *Polymer Single Crystals*, Interscience Publ., New York, 1963, p. 424.
33. J. R. A. Pearson: *Mechanical Principles of Polymer Melt Processing*, Pergamon Press, Oxford, 1966.
34. R. T. Fenner: *Extruder Screw Design*, Iliffe, London, 1970. 34
35. R. T. Fenner: *Principles of Polymer Processing*, Macmillan, London, 1979.
36. Z. Tadmor and I. Klein: *Engineering Principles of Plasticizing Extrusion*, Van Nostrand Reinhold Co., New York, 1970.
37. I. Saltuk, N. Siskovic, and R. G. Griskey, *Polymer Eng. Sci.*, **12 (1972)**, 397, 402.
38. J. G. Savins, *Ind. Eng. Chem.*, **31 (1969)**, 18.
39. R. H. Christopher and S. Middleman, *Ind. Eng. Chem., Fundam.*, **4 (1965)**, 422.
40. R. B. Birds, W. E. Stewart, and E. N. Lightfoot: *Transport Phenomena*, John Wiley & Sons, New York, 1964.
41. R. M. McKinley, H. O. Jalus, W. W. Harris, and R. A. Greenhorn, *A. I. Ch. E., J.*, **12 (1966)**, 17.
42. W. B. Bogarty, Trans. Soc. Petr. Eng., **240 (1967)**, 151. 42
43. D. R. Gregory and R. G. Griskey, *A. I. CH. E., J.*, **13 (1967)**, 122.
44. R. J. Marshall and A. B. Metzner, *Ind. Eng. Chem., Fundam.*, **6 (1967)**, 393.
45. D. L. Dauben and D. E. Manzie, *Trans. Soc. Petr. Eng.*, **240 (1967)**, 1065.
46. E. Burcik, *Earth Mineral Sci.*, **37 (1968)**, 57.
47. W. Kozicki, C. J. Hsu, and C. Tiu, *Chem. Eng. Sci.*, **37 (1968)**, 487.
48. Z. K. Walczak, *unpublished results*, 1964-68.
49. E. H. Wissler, *Ind. Eng. Chem., Fundam.*, **10 (1971)**, 411.

50. J. C. Maxwell, *Phil. Trans. Royal Soc. (London)*, **157 (1867)**, 49.

51. G. W. Schael, *J. Appl. Polymer Sci.*, **10 (1966)**, 653. 51.

52. J. F. Archard, *Proc. Royal Soc. (London)*, **243 (1958)**, 190.

53. R. F. King and D. Tabor, *Proc. Phys. Soc., (London)*, **B65 (1953)**, 728.

54. G. A. Gol'ubyev, L. A. Balyasnikov, and KH. Z. Regelman, *Khim Vol'okna*, **(1968)**, 60.

55. M. M. Denn, *Ind. Rng. Chem. Res.*, **35 (1996)**, 2842. 55

56. A. Szaniawski and A. Zachara, *Polimery* (in Polish), **19 (1974)**, 143; **20 (1975)**, 87.